

Flexible Nonvolatile Cu/Cu_xO/Ag ReRAM Fabricated Using Ink-Jet Printing Technology

by

Simin Zou

A thesis submitted to the Graduate Faculty of
Auburn University
in partial fulfillment of the
requirements for the Degree of
Master of Science

Auburn, Alabama
May 4, 2014

Keywords: ReRAM, Nonvolatile Memory, Memristor, Flexible Memory, Ink-jet Printing

Copyright 2014 by Simin Zou

Approved by

Michael C. Hamilton, Chair, Assistant Professor of Electrical and Computer Engineering
Guofu Niu, Alumni Professor of Electrical and Computer Engineering
Robert Dean, Associate Professor of Electrical and Computer Engineering

Abstract

The design and fabrication of flexible Cu/Cu_xO/Ag ReRAM devices is presented in this work. We have investigated Cu/Cu_xO/Ag capacitor-like structure which exhibits bipolar resistive switching behavior under low-range direct current sweep in the temperature range from 255K to 355K. Ink-jet printing technology is used to fabricate the device. The device displays a resistive switching ratio of more than 30 between high resistance state and low resistance state at room temperature. The device displays a resistive switching ratio of more than 20 between HRS and LRS over 100 cycles. Memory states are reproducible and remained over 500 times. The device has the ability to operate well after over 1000 flexes. The good ductility of printed silver and electroplated copper electrodes and simple cross-point structure of the memory cell result in good flexibility and mechanical robustness, which indicates great potential for future flexible memory applications.

The physical mechanism of Cu/Cu_xO/Ag ReRAM is also presented. The temperature-dependent I-V measurement and cell-size dependent test reveal that the bipolar resistive switching behavior is attributed to the formation and rupture of the conducting filament paths in the insulating material. Furthermore, a resistive switching physical model of the device is presented.

Acknowledgments

First and foremost, the author would like to express her great gratitude and thanks to her academic advisor Dr. Michael C. Hamilton for providing significant guidance, assistance, and financial support throughout this work and her graduate studies. Dr. Niu and Dr. Dean are also thanked for serving in her committee. Their comments and advices are very valuable and helpful.

The author would also like to thank Dr. Michael Bozack for his help with the X-ray photoelectron spectroscopy (XPS) analysis for the Cu_xO thin film and thank Mr. Charles Ellis, Pingye Xu and George A. Hernandez for their assistance in many aspects of this work.

A personal note of appreciation goes to Xiaohui Zou, Yao Ma and Di Zhang for their support, care and love throughout the author's academic endeavors.

Table of Contents

Abstract	ii
Acknowledgments	iii
List of Tables	vi
List of Figures	vii
List of Abbreviations	ix
1 Introduction.....	1
2 Background	5
2.1 Classification of Semiconductor Memory	5
2.2 Resistive Random-Access Memory	8
2.2.1 Classification of Resistive Switching Behaviors	8
2.2.2 Mechanism for Resistive Switching	9
2.2.3 Flexible Resistive Switching Memory Devices	10
3 Fabrication of Cu/Cu _x O/Ag ReRAM Devices	13
4 Device Characterization and Testing	17
4.1 X-ray Photoelectron Spectroscopy	17
4.2 Current-Voltage Characteristics of Cu/Cu _x O/Ag ReRAM Devices	19
4.2.1 Electroforming Process	19
4.2.2 I-V Characteristics after Electroforming	21
4.2.3 Temperature-Dependent I-V Characteristics	23

4.3	Device HRS and LRS Yields.....	24
4.4	Switching Endurance and Data Retention Performance.....	25
4.5	Mechanical Bending Tests and Flex Tests.....	27
4.5.1	Mechanical Bending Tests.....	27
4.5.2	Flex Tests.....	29
4.6	Switching Time Tests	31
5	Resistive Switching Mechanism.....	34
5.1	Non-Cu-Oxidation Control Group.....	34
5.2	Physical Mechanism of Cu/Cu _x O/Ag ReRAM Devices.....	37
5.3	Resistive Switching Mechanism Model.....	43
6	Conclusion and Future Work	45
	References	47
	Appendix A Processing Equipment and Materials	54

List of Tables

Table 4.1	XPS surface elemental composition (at%) versus sputter etching time	19
-----------	---	----

List of Figures

Figure 1.1	Cu/Cu _x O/Ag ReRAM devices fabricated on flexible Kapton substrate.....	4
Figure 1.2	Fabricated Cu/Cu _x O/Ag ReRAM array.....	4
Figure 2.1	Classification of standard semiconductor memories.....	7
Figure 2.2	I-V curves of resistive switching in ReRAM devices	9
Figure 2.3	The conductivity mapping results of TiO ₂ at (a) LRS and (b) HRS	10
Figure 2.4	Photograph of different flexible ReRAM devices.....	12
Figure 3.1	Schematic fabrication flow for the Cu/Cu _x O/Ag ReRAM devices.....	14
Figure 3.2	Photographic process flow for Cu/Cu _x O/Ag ReRAM array	15
Figure 3.3	The SEM image of the cross section of the Cu/Cu _x O/Ag ReRAM device	16
Figure 4.1	The XPS spectra of Cu _x O thin film before sputter etching	18
Figure 4.2	The XPS spectra of Cu _x O thin film after 2 min or 4 min sputter etching	19
Figure 4.3	Electrical forming process and I-V characteristics of the device	21
Figure 4.4	R-V characteristics of the Cu/Cu _x O/Ag ReRAM.....	22
Figure 4.5	Multi-cycle I-V characteristics for the 1st, 250 th and 500 th cycles	23
Figure 4.6	Temperature dependence of I-V curves in semi-log scale	24
Figure 4.7	Distribution of HRS and LRS of fabricated devices	25
Figure 4.8	Switching endurance test of the device during 100 cycles.....	26
Figure 4.9	Data retention performance of the device	26
Figure 4.10	Photograph of the device bent at radius = 11.5mm.....	28

Figure 4.11	Resistance of HRS and LRS as a function of the bending radius	28
Figure 4.12	V_{SET} and V_{RESET} as a function of the bending radius	29
Figure 4.13	Resistance of HRS and LRS during 1~1000 flexes.....	30
Figure 4.14	The Cu/Cu _x O/Ag ReRAM device was bent into a convex shape	30
Figure 4.15	Switching time measurements of (a) RET and (b) RESET operation.....	32
Figure 5.1	Hysteretic I-V behavior of the Cu/Cu _x O/Ag ReRAM device	35
Figure 5.2	I-V curve of a non-oxidation device.....	35
Figure 5.3	Resistance dependence of HRS and LRS on number of switching cycles.....	36
Figure 5.4	Temperature dependence of HRS, IRS and LRS	38
Figure 5.5	Temperature-dependent I-V characteristics at HRS in log-log scale	39
Figure 5.6	The LnI versus 1/KT curve for HRS	40
Figure 5.7	Activation energy at various voltages	40
Figure 5.8	Logarithmic plot of I-V characteristic of positive voltage region.....	42
Figure 5.9	Photograph of the fabricated different cell-size ReRAM array.....	42
Figure 5.10	Resistance of HRS and LRS versus cell size of Cu/Cu _x O/Ag ReRAM devices ...	43
Figure 5.11	Schematic diagram of the resistive switching mechanism model.....	44
Figure A.1	FUJIFILM Dimatix Material Printer	54
Figure A.2	Kapton polyimide substrate	54
Figure A.3	Silver nanoparticle ink.....	55
Figure A.4	Hot plate	55
Figure A.5	YES (Yield Engineering Systems) vacuum cure oven.....	56
Figure A.6	Copper electroplating equipment.....	56
Figure A.7	Keithley 4200 (Semiconductor Characterization Systems) parameter analyzer ..	57

Figure A.8 Micro-manipulated cryogenic probe system 57

List of Abbreviations

BRS	Bipolar Resistive Switching
HRS	High Resistance State
IRS	Initial Resistance State
LRS	Low Resistance State
MOM	Metal-Oxide-Metal
RAM	Random-Access Memory
ReRAM	Resistive Random-Access Memory
ROM	Read-Only Memory
SEM	Scanning Electron Microscope
URS	Unipolar Resistive Switching

Chapter 1

Introduction

In the modern world, semiconductor nonvolatile memory devices, such as programmable read-only memory (PROM) and Flash memory, have been successfully scaled down to achieve high-capacity memories by perfecting the lithography technology. However, how to satisfy the increasing demand for the scaling of conventional memory devices is the most serious problem encountered due to the physical limitation. Compared to conventional memories, ReRAMs have attracted wide attention due to their various characteristics, such as high switching speed, high data density, low power consumption, excellent scalability and simple structure. ReRAMs have been regarded as one of the promising candidates of the next generation nonvolatile memory. Moreover, ReRAMs have neuromorphic and biological circuit applications, signal processing and programmable logic applications.

A ReRAM device consists of a two-terminal metal-oxide-metal (MOM) sandwich cross structure. Scientists such as Leon Chua has pointed that all two-terminal nonvolatile memory devices including ReRAM should be considered memristors, which are the missing non-linear passive electrical components relating electric charge (Q) and magnetic flux linkage (Ψ). There are two kinds of resistive switching behaviors reported in ReRAM, which are unipolar resistive switching (URS) and bipolar resistive switching (BRS). The switching direction of URS depends on the applied voltage amplitude whereas BRS depends on the polarity of the applied voltage. The capacitor-like memory cell is characterized by four resistive states: initial resistance state

(IRS), electroformed resistance state (ERS), high resistance state (HRS) and low resistance state (LRS). Reversible resistive switching between HRS and LRS can be achieved by applying either a current or a voltage bias to the memory cell. The MOM cell shows hysteretic current-voltage (I-V) characteristics and this hysteretic behavior keeps the resistive switching in HRS or LRS unless the voltage bias reaches or exceeds the threshold voltages, which are called RESET voltage and SET voltage, respectively. Since most of resistive switching materials are insulators, IRS is the most resistive state of other states. For most ReRAM devices, a pretreatment process named electroformed process is essential, leading to a great increase in the conductance by applying a high current or voltage to the memory cell at IRS. Generally, ERS has a low resistance, which is comparable to LRS and IRS has higher resistance than HRS.

Resistive switching is a significant physical effect in the ReRAM operation. The resistive switching effect has been studied for more than 45 years. Research in addressing ReRAM has been investigated by an increasing number of research groups [1-8]. For example, Hewlett-Packard laboratories have studied Pt/Organic monolayer/Ti memory devices with a tunable resistor more than 10^2 - 10^5 Ω range under current or voltage control [2]. Gergel-Hackett, et al. have investigated flexible Al/TiO₂/Al solution-processed memory devices with an ON/OFF ratio of greater than 10000:1 and long data retention time of over 1.2×10^6 s [3]. Jin-Woo Han, et al. fabricated resistive switching function embedded e-textile with Cu/Cu_xO/Pt sandwich structure [4].

Up to now, various resistive switching models have been suggested, including filament-type model [5], space charge limited current (SCLC) model [6], Schottky barrier model [7], oxygen migration model [8] and so on. However, these physical mechanisms cannot completely explain the universal resistive switching characteristics.

In this research, we have investigated the characterization of the BRS in Cu/Cu_xO/Ag (1<x<2) memory devices for flexible ReRAM applications. Our measurements consist of two-point probe DC measurement. The material we used to fabricate memory devices are copper and silver, which are relatively abundant in the natural world. We use ink-jet printing technology during the fabrication process which has extensive potential for roll-to-roll processing in industrial production. In addition, the entire fabrication processing we used is low temperature processing, which are lower than 200 °C. Kapton polyimide film is used as the substrate, allowing a good flexibility of the memory devices. Fig 1.1 shows a photograph of fabricated Cu/Cu_xO/Ag memory cells at the bending condition. Fig 1.2 shows the Cu/Cu_xO/Ag ReRAM array.

The fabricated ReRAM devices have the characteristics of high resistive switching repeatability of more than 500 times, low-voltage operation (less than 1 V), reliable switching endurance of over 100 cycles, data retention for nearly 2 weeks, low-temperature fabrication, HRS/LRS ratio of greater than 20 under room temperature and operated well after being flexed over 1000 times. Furthermore, to explore the physical mechanism of the BRS characteristics in the device, temperature dependence of resistive switching and cell-size dependent measurement have been investigated, which reveals the conductive filament path has the most probability to lead to the BRS behavior of Cu/Cu_xO/Ag ReRAM devices.

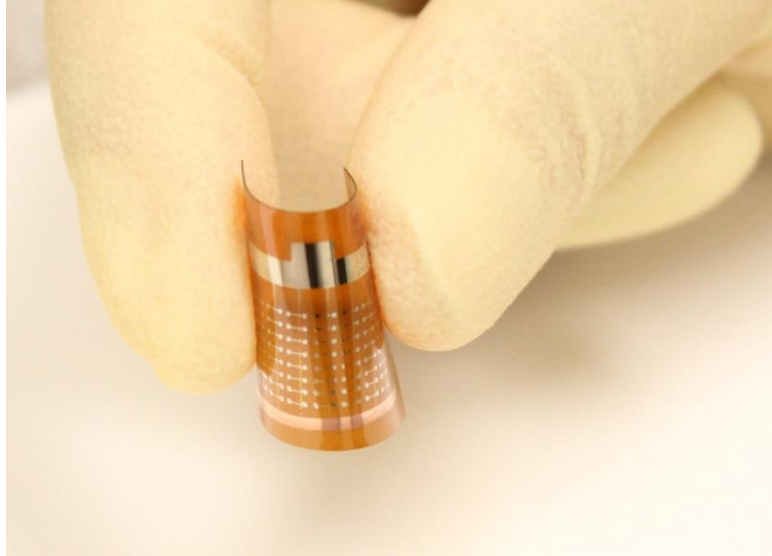


Figure 1.1: Cu/Cu_xO/Ag ReRAM devices fabricated on flexible Kapton substrate.

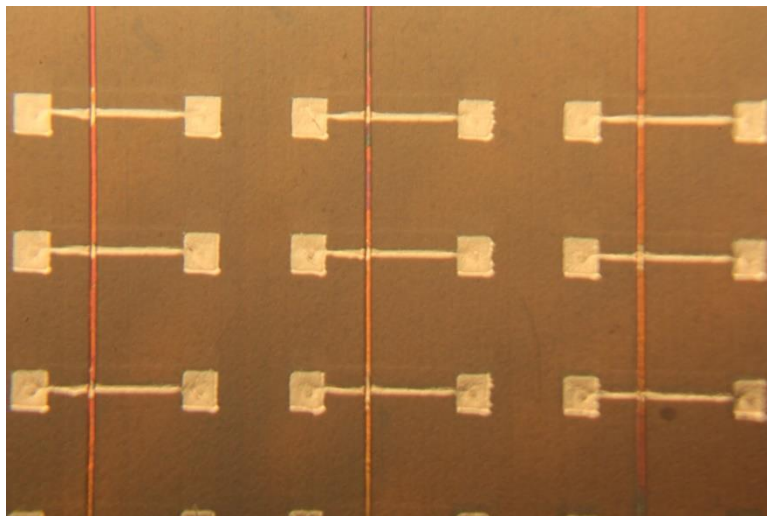


Figure 1.2: Fabricated Cu/Cu_xO/Ag ReRAM array

Chapter 2

Background

2.1 Classification of Semiconductor Memory

As an important electronic data storage device, semiconductor memories have sustained increasing advances in the integrated circuit technologies. In addition, portable electronics are heavily reliant on the development of the fast-speed, high-density, low-power consumption low-cost and simple-manufacture-technique memories. Basically, semiconductor memories can be divided into random access memories (RAMs) and read-only memories (ROMs). Compared to RAMs, ROMs are designed to hold permanent data and instead of being written to, ROMs are normally read-only.

RAMs can be further classified as volatile RAMs and nonvolatile RAMs. The volatile RAMs include dynamic RAMs (DRAMs) and static RAMs (SRAMs) and the volatile RAMs lose stored data once the power to the memory chip is down. DRAMs are usually used as the main memory in the computer for their feature of high density and low cost. SRAMs are faster and less memory refresh required, which are mostly used for cache memories in the computer. Depending on different materials or operating principles, nonvolatile RAMs are classified as ferroelectric RAMs (FeRAMs) [9], magnetoresistive RAMs (MRAMs) [10], phase-change RAMs (PRAMs) [11], flash memory and resistive RAMs (ReRAMs) [1-8]. FeRAM is a kind of RAM which has similar construction to DRAM. However, FeRAM has a thin film of ferroelectric material (lead zirconate titanate) different from the dielectric layer in a DRAM.

Compared to conventional RAMs, MRAMs store data by magnetic storage elements not current flow or electric charge. The magnetic storage element is formed by two ferroelectric plates, holding two magnetic fields and sandwiching an insulating layer. PRAM is also known as PCRAM and C-RAM, exploiting its unique characteristics of chalcogenide glass. ReRAMs have cross-point architecture and a fairly large number of organic and inorganic material systems show resistive switching effects. The physical mechanism of ReRAMs have not been explained clearly now. Mechanism model such as filament-like model [5], oxygen migration model [6], Schottky barrier model [7], space charge limited current (SCLC) model [8] have been published.

ROMs can be classified as mask ROMs (MROMs), programmable ROMs (PROMs), erasable programmable ROMs (EPROMs), electrically erasable programmable ROMs (EEPROMs) and ultraviolet erasable EPROMs (UVEEPROMs). Fig 2.1 shows the categories of semiconductor memories.

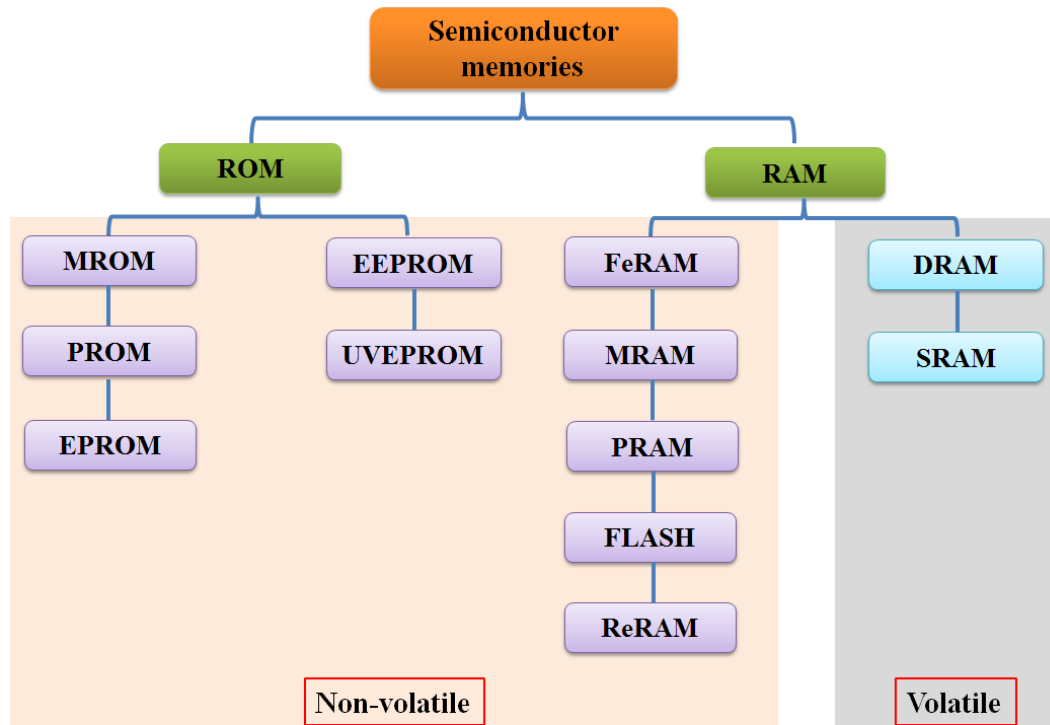


Figure 2.1: Classification of standard semiconductor memories.

2.2 Resistive Random-Access Memory

ReRAM is a kind of emerging nonvolatile memory. It is based on various new materials, such as organic compounds [2], metal oxide [3, 4], showing a resistive switching behavior. The ReRAM memory cells have a capacitor-like architecture composed of semiconducting or insulating material sandwiched between top and bottom electrodes.

Hysteretic current-voltage (I-V) characteristic in metal-oxide-metal (MOM) structure of Al/Al₂O₃/Al was first published by T. W. Hickmott in the year 1962 [12]. His research indicated that resistive switching was induced by the applied electric fields. Since then, a variety of metal oxides have been subsequently reported showing resistive switching, such as TiO₂ [3], NiO [13, 14] and so on.

2.2.1 Classification of Resistive Switching Behaviors

The resistive switching behavior of the ReRAM can be categorized into two types: BRS and URS. In BRS, the resistive switching depends on the polarity of the applied voltage bias. This type of resistive switching behavior occurs with various semiconducting oxides, such as: HfO₂ [15], Cu_xO [16], SrTiO₃ [17], Ta₂O₅ [18], Pr_{0.7}Ca_{0.3}MnO₃ [19], Si₃N₄ [20], Nb₂O₅ [21], CeO₂ [22]. In URS, the resistive switching direction relies on the amplitude of the applied voltage bias. In other words, the different resistance states of the system can be switched by application of continuous electric stress of the same or the opposite polarities. The URS has been reported in materials such as: CoO [23], SnO₂ [24], MgO [25], Lu₂O₃ [26] and so on. Interestingly, materials such as: TiO₂ [27], ZnO [1, 28], BST [29], NiO [13, 14], ZrO₂ [30], YMnxO₃ [31] have been observed exhibiting the coexistence of BRS and URS. Fig 2.2 shows

the I-V characteristics of URS in a Pt/NiO/Pt memory cell [32] and BRS in a Al/TiO₂/Al memory cell [3].

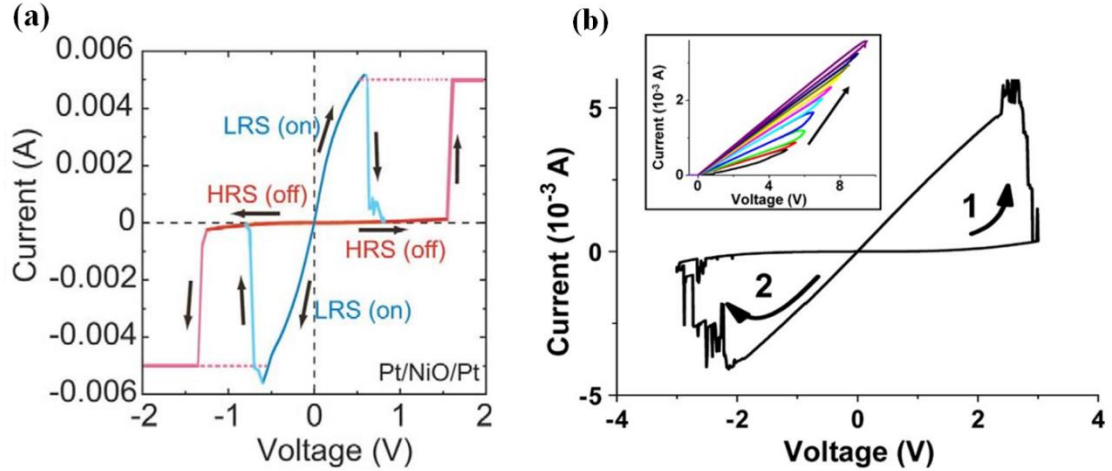


Figure 2.2: I-V curves of resistive switching in ReRAM devices. (a) URS in a Pt/NiO/Pt cell [32]. (b) BRS in a Al/TiO₂/Al cell [3].

2.2.2 Mechanism of Resistive Switching

The physical origin of the resistance variation in the resistive switching materials is not fully understood yet, despite the fact that this variation is observed in every ReRAM reported. Generally, there are two basic driving mechanism, one is filament-type resistive switching, the other is interface-type resistive switching.

In filament-type resistive switching mechanism, the resistive switching is attributed to the formation and rupture of the conductive filament paths in the insulating material. The filament-type resistive switching model was first published in 1967 by J. G. Simmons and R .R. Verderber [33]. In some previous works, high spatial resolution provided the evidence of the formation and rupture of the conductive paths [34, 35]. Fig 2.3 shows the conductivity mapping results of TiO₂ films at LRS and HRS by using HVAFM (high vacuum atomic force microscopy). Conductive

spots can be observed clearly in the electroforming process SET process. In the Cu/ZrO₂:Cu./Pt memory cell, by conducting temperature-dependent measurements, Guan, et al. investigated Cu conductive bridge as the conductive filament path is formed in the SET process and the dissolving of the existing Cu conductive bridge is caused by the Joule heating assisted oxidation [36].

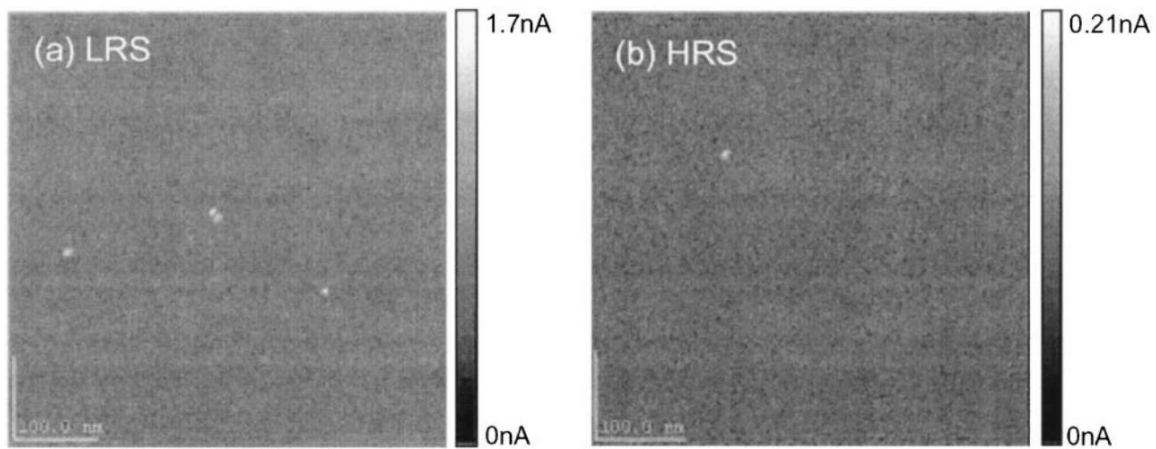


Figure 2.3: The conductivity mapping results of TiO₂ at (a) LRS and (b) HRS [35].

In interface-type resistive switching mechanism, the resistive switching is caused by the change of charge carriers or mobile ions which contribute to current transport. Various models have been proposed for physical mechanism involving an interface-type conductive path, including: (electrochemical) migration of oxygen vacancies [6, 37, 38], trapping and detrapping of charge carriers (electrons or holes) [39] and Schottky barrier model [7, 40].

2.2.3 Flexible Resistive Switching Memory Devices

Flexible electronics systems such as wearable electronics and built-in elements have become an emerging field. Based on this trend, the demand for a flexible memory will also increase to support flexible electronics. Flexible ReRAM has been demonstrated to be a promising technology by several research groups.

For instance, Sungho et al., implemented Al/TiO_x/Al ReRAM fabricated on transparent and flexible substrate of polyethersulfone (PES) [41]. The I-V correlation of this ReRAM follows the SCLC theory. Meanwhile, Yongsung et al., implemented a 8×8 crossbar array of organic ReRAM devices on polyethylene terephthalate (PET) flexible substrate [42]. This group studied HRS/LRS ratio as a function of the bending radius as well as the number of bendings. The authors of this work noted there were no significant difference in the HRS/LRS ratio regardless the bending radius and the cycles. Furthermore, Lu-Hao et al., fabricated graphene oxide resistive switching memories on PET with high RESET speed of 100 ns and a SET speed of approximately 100 μs [43]. The above flexible ReRAM devices are shown in Fig 2.4.

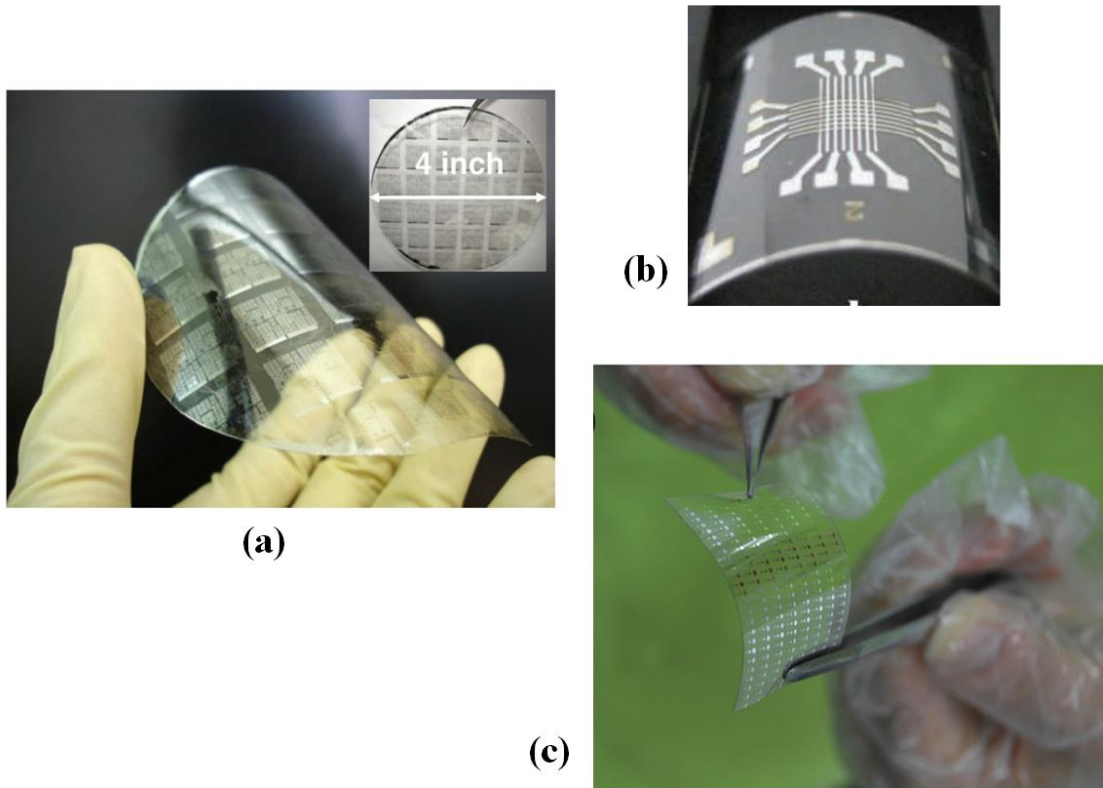


Figure 2.4: Photograph of different flexible ReRAM devices. (a) The Al/TiO_x/Al ReRAM [41]. (b) Ti/Au/Al/PI:PCBM/Al organic memory devices [42]. (c) Graphene oxide based ReRAMs [43].

Chapter 3

Fabrication of Cu/Cu_xO/Ag ReRAM Devices

The Cu/Cu_xO/Ag ReRAM Device was fabricated on Dupont Kapton polyimide substrate. A silver thin film seed layer was printed on Kapton substrate. Ink-jet printing was performed using a FUJIFILM Dimatix Material Printer 2831 with a piezoelectric print head cartridge. The ink used in this work was U5603 from Sun Chemical (20 wt% suspension of silver nanoparticles dispersed in ethanol and ethanediol, particles size < 150 nm).

After printing, the sample was thermally cured at 200 °C for 2 h in a nitrogen environment to remove solvent and other impurities from the printed silver ink. Copper was electroplated on the silver lines at a current density of approximately 6 mA/cm² for 5 min. We used a copper plating solution consisting of sulfuric acid (100 g/L), copper sulfate (60 g/L), Enthone SC MD (8 ml/L), hydrochloric acid (2 ml/L), and Enthone SC Lo (2 ml/L). The copper coated sample was placed on a hot plate in air with heating temperature of 200 °C for 3 h to create a thin oxide (Cu_xO) layer on the Cu. Note that we also fabricated a subset of control samples that did not undergo the Cu oxidation step. Next, a second nanoparticle silver film pattern was printed on top of the Cu_xO layer to create the cross structure of the device as well as Ag top electrodes (TE). This layer was thermally cured at 200 °C for 2 h in a nitrogen environment. Last, a cotton swab with 1 % HCl solution was used to remove the copper oxide thin layer in a region away from the Ag overlay to allow better connection to the Cu bottom electrode (BE) [43]. Note that more information of the fabrication equipment and materials can be found in Appendix A. The

fabrication process flow is schematically shown in Fig 3.1. Fig 3.2 shows the photograph of the fabrication process flow. The SEM image of the cross-sectional view of the Cu/Cu_xO/Ag MOM device fabricated on a Kapton substrate is shown in Fig 3.3.

The memory cell has a cell size of 20 μm×20 μm, which is the smallest deposit feature limit of the cartridge. In the cell-size dependent test, different cell-size memory devices have also been fabricated in the same process. The ink-jet printer we used is the FUJIFILM DMP (Dimatix Material Printer) 2831 with a piezoelectric print head cartridge.

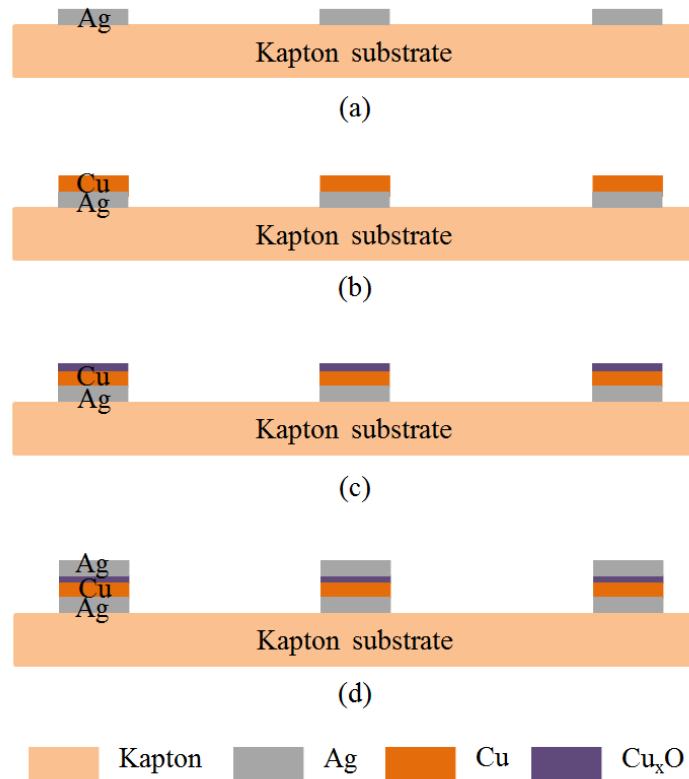


Figure 3.1: Schematic fabrication flow for the Cu/Cu_xO/Ag ReRAM devices. (a) Silver seed layer printed. (b) Electroplated copper. (c) Cu_xO layer created. (d) Silver top electrode printed.

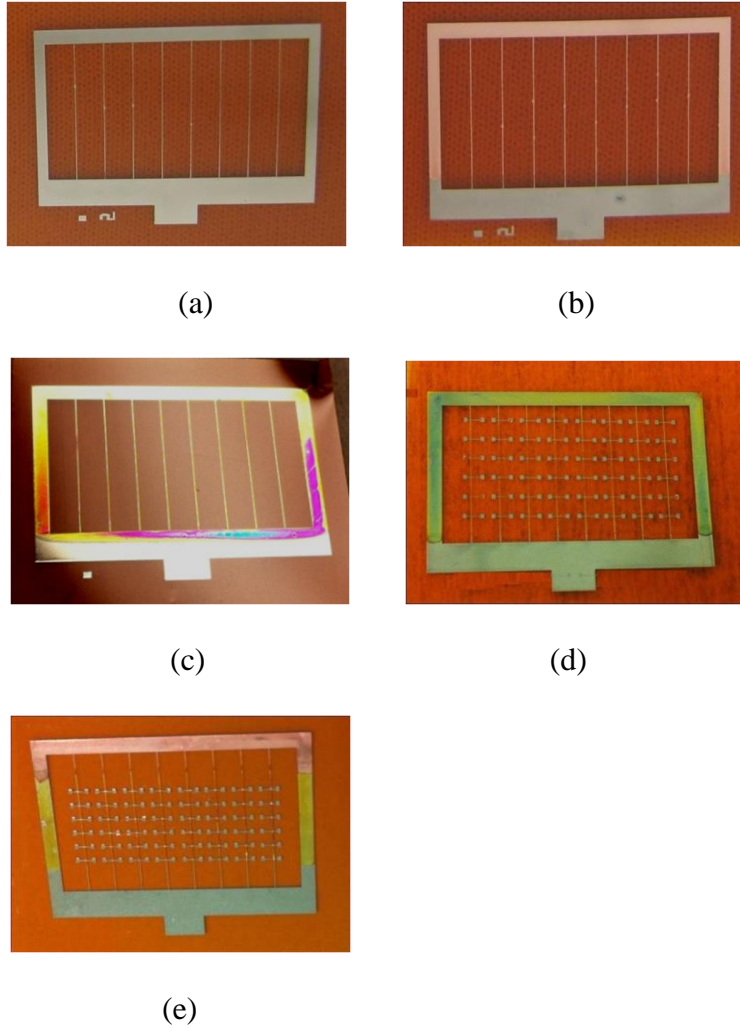


Figure 3.2: Photographic process flow for Cu/Cu_xO/Ag ReRAM array. (a) Ink-jet printed silver seed layer. (b) Electroplated copper lines. (c) Copper oxidation. Create a thin Cu_xO layer on the copper. (d) Ink-jet printed silver top electrodes (TE). (e) Copper bottom electrodes (BE) created by removing copper oxide.

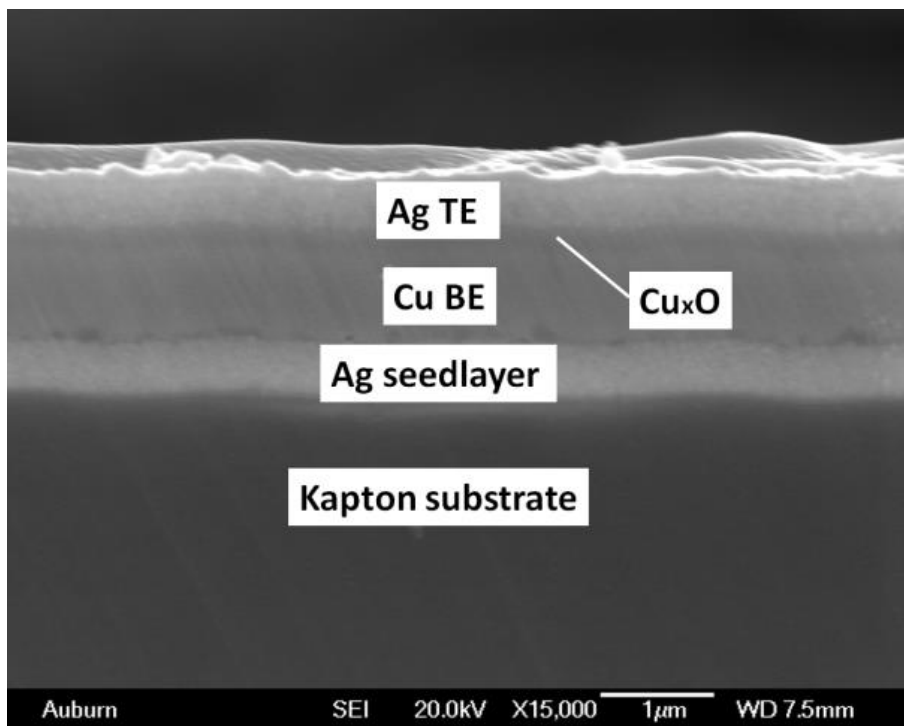


Figure 3.3: The SEM image of the cross section of the Cu/Cu_xO/Ag ReRAM device.

Chapter 4

Device Characterization and Testing

4.1 X-ray Photoelectron Spectroscopy

X-ray photoelectron spectroscopy is one of the most common tools for thin film characterization. To analyze the oxide material induced BRS behavior, we did X-ray photoelectron spectroscopy (XPS) on the original Cu_xO surface and the same sample after sputter etching for 2 min and 4 min.

Fig 4.1 shows the X-ray photoelectron spectroscopy (XPS) of the original oxide film before sputter etching, using a sputter rate of $25 \text{ \AA}/\text{min}$. The calculated XPS surface element composition (at %) versus sputter time (depth) is shown in Table 4.1. For the initial Cu_xO film, high resolution scans over the $\text{Cu}2p$ peak in the XPS spectra indicate a native Cu oxide state, which is a CuO film. This is corroborated by the approximately 50/50 at% Cu/O elemental ratio of the “as received” surface.

However, as shown in Fig 4.2, over the sputtered depth of $\sim 100 \text{ \AA}$, there is a transition from native CuO to $\text{Cu}_2\text{O}/\text{Cu}$, shown by the shape change in the $\text{Cu}2p$ peak and accompanying $\text{Cu}2p_{3/2}$ binding energy changes observed in the spectra. Additionally, the layer composition shows an increase in Cu with depth. This indicates that the copper oxide has transitioned from CuO to $\text{Cu}_2\text{O}/\text{Cu}$ over a film thickness of $\sim 100 \text{ \AA}$. We say “ $\text{Cu}_2\text{O}/\text{Cu}$ ” due to the well-known limitation of XPS to distinguish $\text{Cu}(0)$ = elemental and $\text{Cu}(I)$ = Cu_2O , since the $\text{Cu}2p_{3/2}$ $\text{Cu}(0)$ and $\text{Cu}(I)$ peak shapes and binding energies are nearly identical [44]. Since the Cu_xO thickness,

indicated by Fig 3.3, is on the order of 0.1 micron = 1000Å, we presume we have not yet reached the Cu substrate and that the Cu2p feature at a depth of ~100Å is largely Cu₂O.

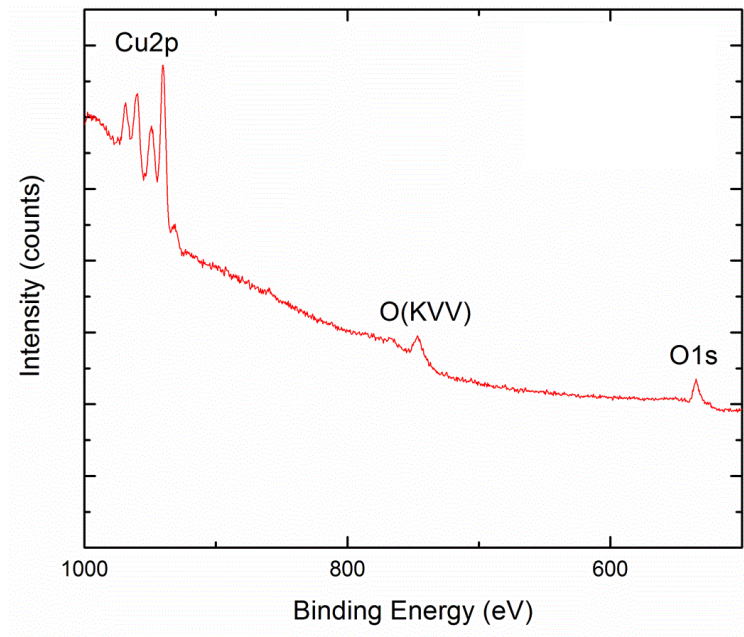


Figure 4.1: The XPS spectra of Cu_xO thin film before sputter etching.

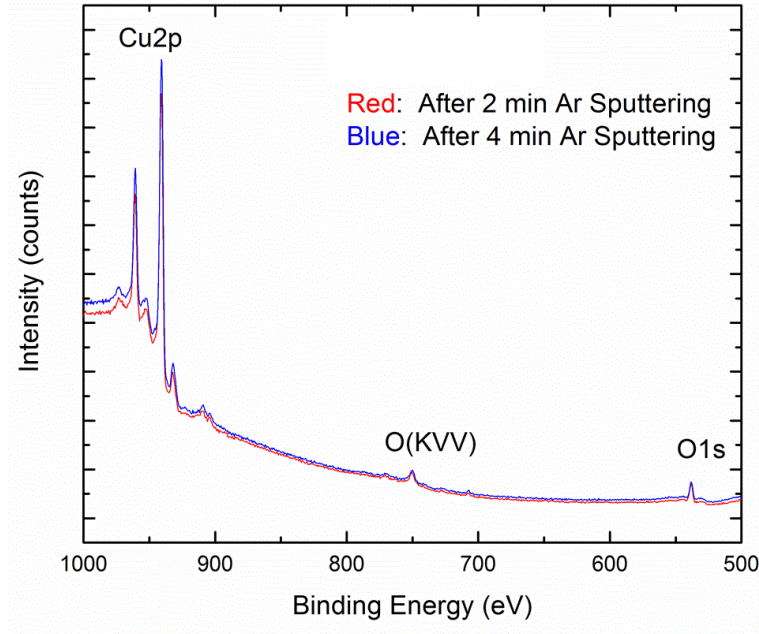


Figure 4.2: The XPS spectra of Cu_xO thin film after 2 min or 4 min sputter etching. (Corresponding to removal of ~50/100Å of the initial Cu_xO surface).

Time (min)	Cu (%)	O (%)
0	47.9	52.1
2	63.7	36.3
4	69.6	30.4

Table 4.1: XPS surface elemental composition (at%) versus sputter etching time.

4.2 Current-Voltage Characteristics of Cu/Cu_xO/Ag ReRAM Devices

4.2.1 Electroforming Process

Electroforming process is a pretreatment procedure for resistive switching in most binary-transition-oxide ReRAM such as TiO₂ [27], ZnO [1] and NiO [45]. These ReRAMs show

electrically insulating characteristics initially, with relatively high resistance. For different ReRAM devices, by applying high electrical stress (a voltage or a current) to one of the two electrodes (TE or BE), the resistance of the device can be decreased by several orders of magnitude (corresponding to a dramatic increase in current) suddenly. The specific voltage/current which causes this sudden change is called the electroforming voltage/current or threshold voltage/current. The electroforming procedure plays a significant role in resistive switching. In some literatures, electroforming is believed to activate resistive switching in the switching material layer and lead to the formation or growth of some conductive objects such as filaments [46].

In this work, a Keithley 4200 semiconductor characterization system was used to measure the current-voltage (I-V) characteristics of the fabricated devices. The electroforming process is labeled as (1) in the Fig 4.3 [47]. By applying a voltage sweep from 0 V to +2 V as the arrow shows, a large increase (corresponding to a dramatic reduction in resistance) happens in the memory cell's current at approximately +1.8 V (the electroforming voltage), indicating that the strong electrical stress leads to the formation of conducting filaments.

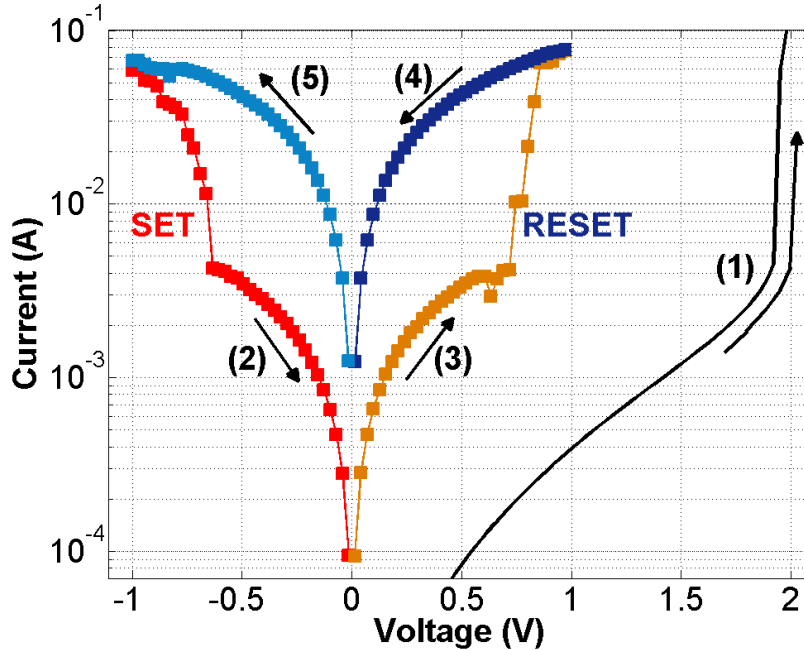


Figure 4.3: Electrical forming process and I-V characteristics of the memory.

4.2.2 I-V Characteristics after Electroforming

Voltage sweeps were performed in lower range. In the Fig 4.3, the arrows indicate the voltage sweeping direction ($-1\text{ V} \rightarrow 0\text{ V} \rightarrow +1\text{ V} \rightarrow 0\text{ V} \rightarrow -1\text{ V}$), the I-V hysteresis curve is obtained. During the voltage scan from -1 V to -0.8 V (SET voltage), a sharp current decrease is observed before step (2), which is called the SET process, resulting in a significant change of resistance in the ReRAM memory cell from the low resistance state (LRS) to the high resistance state (HRS). Next, when the sweeping voltage increases to $+0.8\text{ V}$ (RESET voltage), a rapid increase in current is observed at the end of step (3), which is called the RESET process. During the RESET process, the resistance of the ReRAM device is switched from HRS to LRS. The magnitudes of both the SET voltage and the RESET voltage are less than 1 V , which shows the low-voltage operation feature of the $\text{Cu}/\text{Cu}_x\text{O}/\text{Ag}$ memory devices.

Fig 4.4 shows the corresponding resistance-voltage (R-V) curve during the same voltage sweep. Two resistance states (HRS and LRS) are demonstrated. When the voltage reaches the V_{SET} , the resistance state of the device is switched to HRS. Alternatively, LRS is achieved after the voltage bias reaches V_{RESET} . The resistance at HRS and LRS is approximately $150\ \Omega$ and $10\ \Omega$ with a ratio of 15.

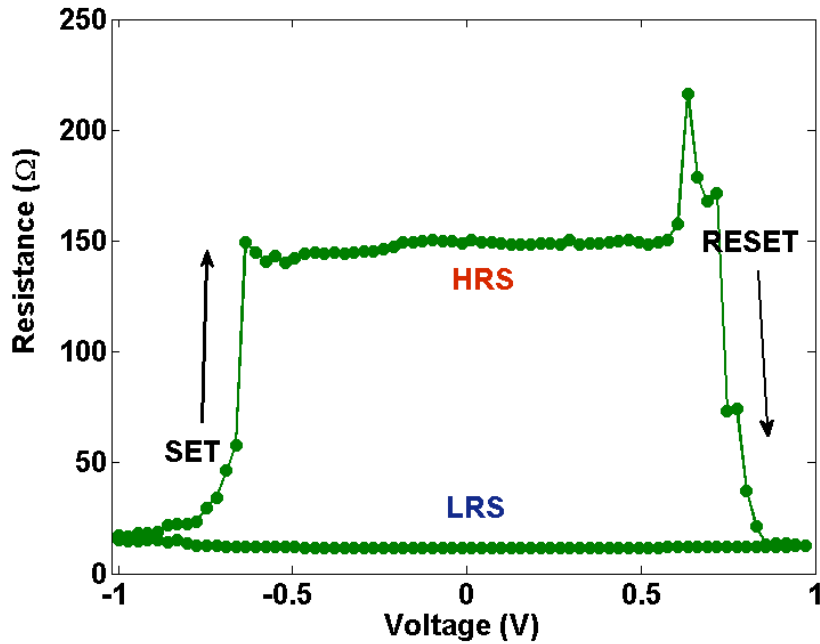


Figure 4.4: R-V characteristics of the Cu/Cu_xO/Ag ReRAM.

The device shows excellent reproducible behavior, as shown in Fig 4.5. The measurement was conducted in a lab environment at room temperature. The arrows indicated the sweeping direction, which starts from -1 V to +1 V then back to -1 V. During all of the voltage sweeps, the I-V curves show reproducible and stable behavior, and the ratio of HRS/LRS is almost constant.

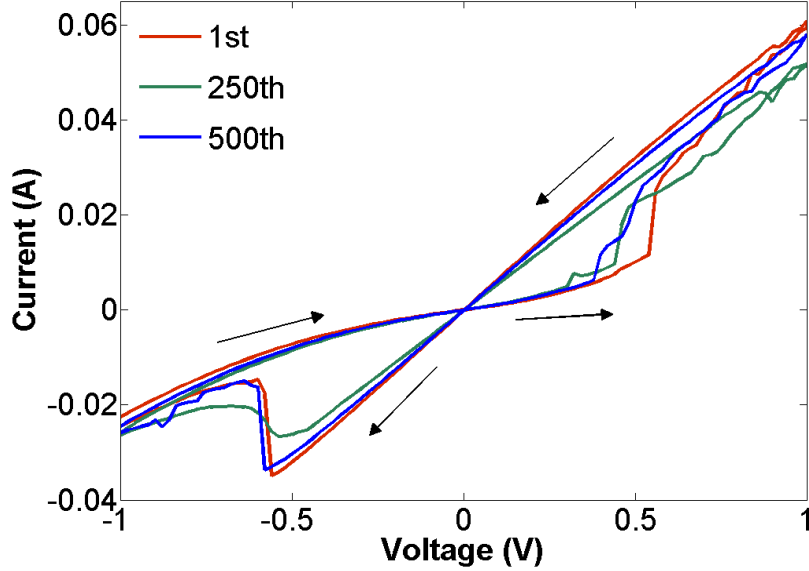


Figure 4.5: Multi-cycle I-V characteristics for the 1st, 250 th and 500 th cycles.

4.2.3 Temperature-Dependent I-V Characteristics

Temperature dependence of BRS characteristics after electroforming is investigated, which is shown in Fig 4.6. The temperature-dependent measurement was conducted in a micro-manipulated cryogenic probe station. The workable temperature range of the cryogenic probe station is from 11 K to 370 K. However, an excessive high or cold temperature can affect proper functioning of the ReRAM device. When the temperature is above 365 K or below 250 K, the ReRAM device does show BRS behavior. In Fig 4.6, the temperature range is from 255 K to 315 K with a step size of 15 K. No strong temperature dependence was observed for the switching voltages V_{SET} and V_{RESET} , which are approximately -0.6 V and +0.6 V respectively.

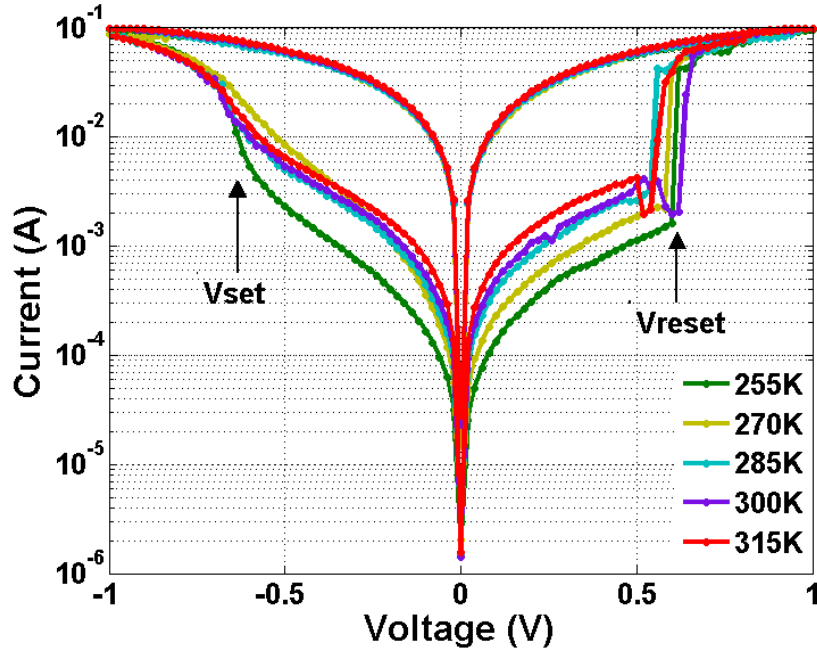


Figure 4.6: Temperature dependence of I-V curves in semi-log scale.

4.3 Device HRS and LRS Yields

We have fabricated and electrically tested more than 220 devices. From 121 functional memory cells, the HRS yield and LRS yield are shown in the Fig 4.7. The average value of resistance at HRS and LRS is 95.3Ω and 13.7Ω , respectively. There is no overlap between HRS and LRS and the ratio of HRS and LRS is approximately 6.9. The variation of the resistance at HRS and LRS might be caused by: (a) the thickness of Cu_xO film was not perfectly uniform and (2) the defect in the fabrication processing.

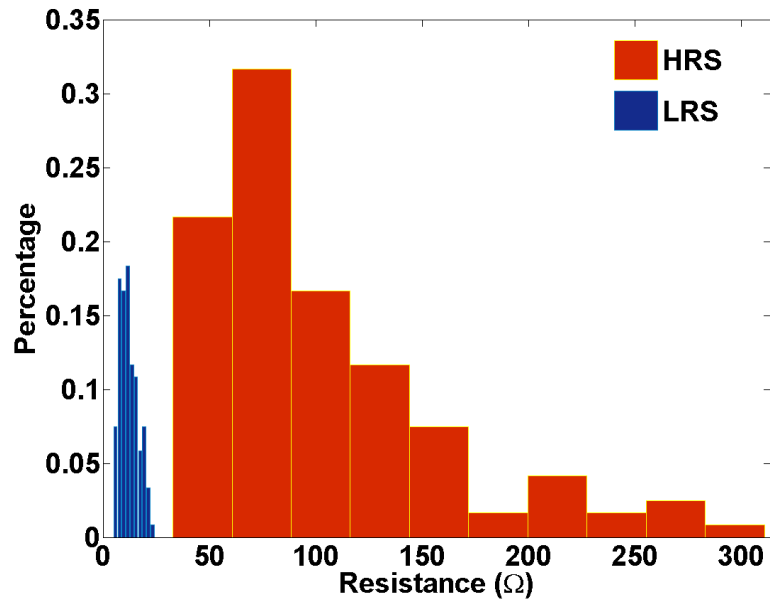


Figure 4.7: Distribution of HRS and LRS of fabricated devices.

4.4 Switching Endurance and Data Retention Performance

The switching endurance and data retention characteristics were studied to evaluate the reliability of the Cu/Cu_xO/Ag ReRAM devices. Fig 4.8 shows the data endurance at 295 K. For the switching cycle measurements, -0.8 V and +0.8 V were applied to the device as the SET voltages and RESET voltages, respectively, switching the device to HRS and LRS. Since once the device is switched to one state (i.e. HRS/LRS), the resistance of the device will not be changed until the voltage bias reaches to RESET voltage/SET voltage to switch the device to LRS/ HRS. The resistance of the device can be read at a low voltage range. In this study, the resistances of HRS and LRS were recorded at low voltage range from -0.01 V to +0.01 V. During 100 switching cycles, resistance value of HRS was approximately 120 Ω and LRS was around 6 Ω without switching failure. The resistance value of HRS and LRS remained stable with a ratio of 20. Fig 4.9 shows the retention characteristics of the device at room temperature.

After switching the device to one resistive state (HRS or LRS), no electrical power was needed to maintain the resistance in this state. As shown in Fig 4.9, no significant change of the resistance at both HRS and LRS remained for nearly 2 weeks, which further proved the nonvolatile nature of the Cu/Cu_xO/Ag ReRAM device.

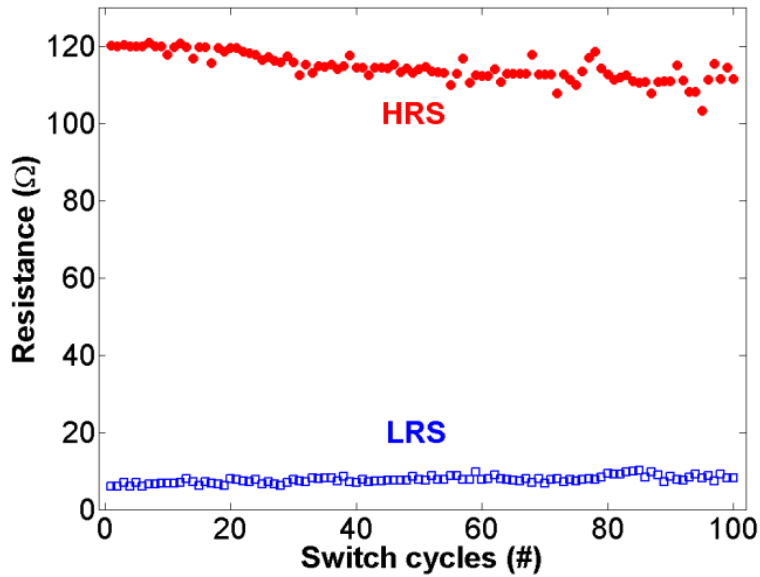


Figure 4.8: Switching endurance test of the device during 100 cycles.

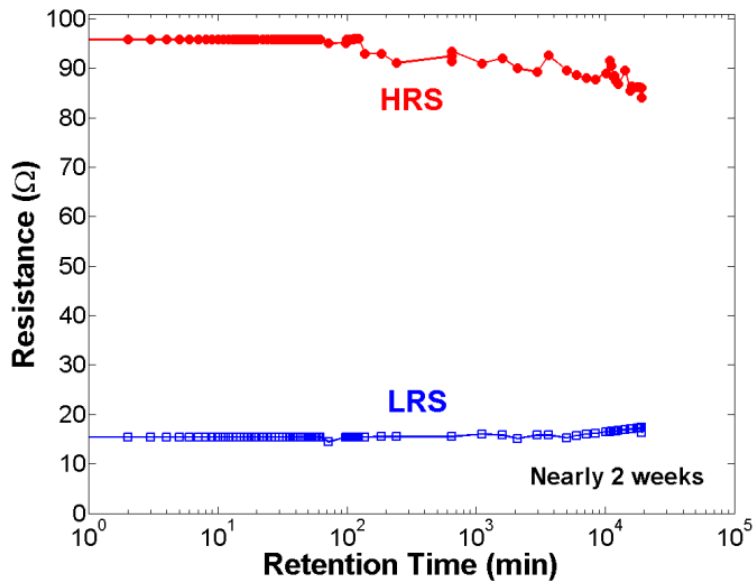


Figure 4.9: Data retention performance of the device.

4.5 Mechanical Bending Tests and Flex Tests

Flexibility is very important for future electronic applications such as wearable electronic devices. The mechanical robustness test and flex tests of the Cu/Cu_xO/Ag ReRAM devices were performed in order to examine the mechanical stability of the devices. Thus, excellent electrical characteristic under bending condition is crucial for practical flexible electronic devices. This required property of our Cu/Cu_xO/Ag memory cells was investigated in detail.

4.5.1 Mechanical Bending Tests

In the mechanical bending tests, I-V measurements were performed under various degree of bending. We investigated the HRS/LRS ratios as a function of the bending radius of the Cu/Cu_xO/Ag memory cells. The device was bent to form a convex shape with different radius of 55 mm, 35 mm, 26 mm, 17.5 mm, 11.5 mm and 5.5 mm and the device was measured while being flexed, which is shown in the Fig 4.10. The devices exhibit stable I-V hysteretic behavior under bending condition. With the increase of curvature, the resistances at HRS and LRS remained stable with a ratio of greater than 7, which is shown in Fig 4.11. In particular, we investigated the distribution of SET voltages and RESET voltages according to the bending radius, which is shown in Fig 4.12. The V_{SET} was at a range from -0.58V to -0.80 V and the V_{RESET} was from +0.67 V to +0.79 V. There was no overlap between SET voltages and RESET voltages observed during the bending process, indicating the device can be controlled precisely and operated well at low voltage, even under significant flexing conditions.

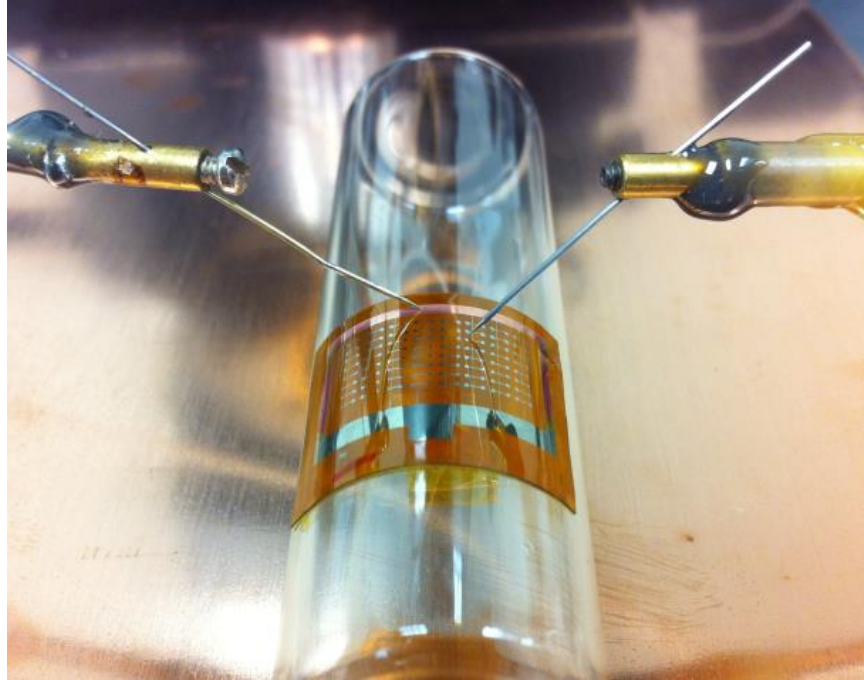


Figure 4.10: Photograph of the device bent at radius = 11.5 mm.

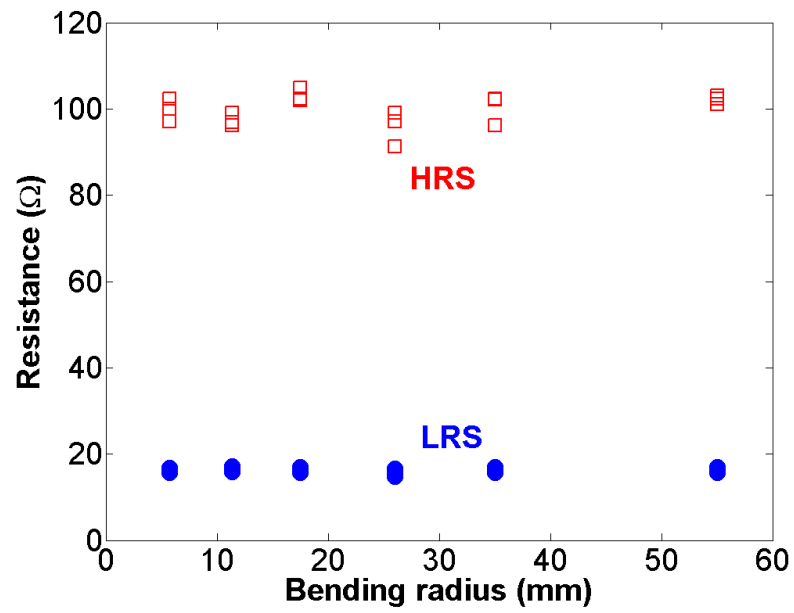


Figure 4.11: Resistance of HRS and LRS as a function of the bending radius.

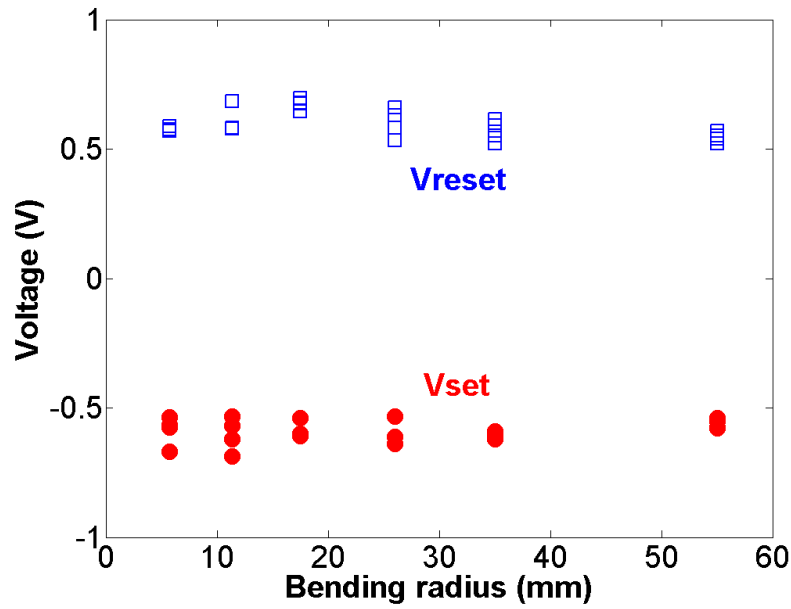


Figure 4.12: V_{SET} and V_{RESET} as a function of the bending radius.

4.5.2 Flex Tests

The statistical data of mechanical robustness test for the Cu/Cu_xO/Ag ReRAM memory cell is shown in Fig 4.13. The device was physically flexed for over 1000 cycles. For each flex cycle, the 25-mm-long device was bent into a convex shape and then into a concave shape with a radius of 8mm (convex shape shown in Fig 4.14). During 1000 flex cycles, the ratio of HRS and LRS was approximately 20 and remained relatively stable.

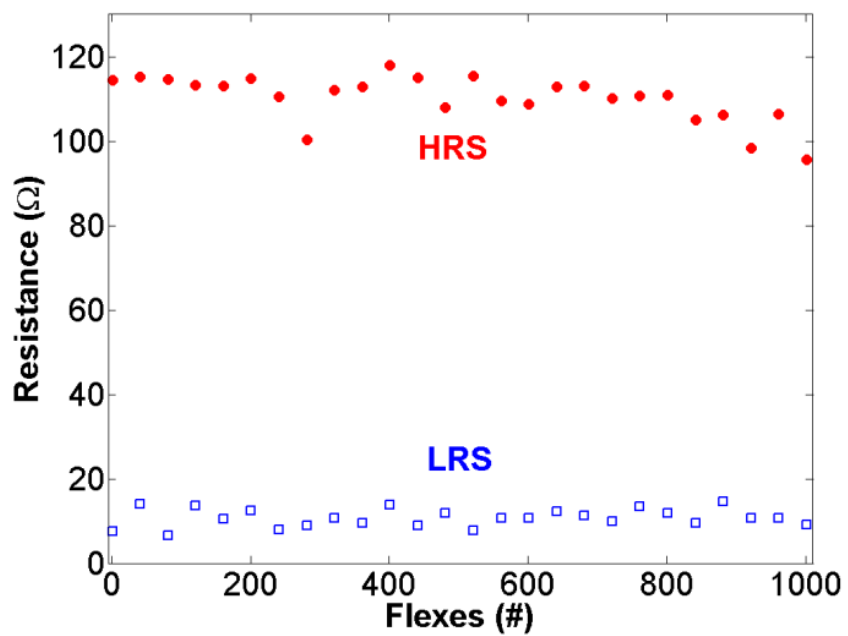


Figure 4.13: Resistance of HRS and LRS during 1~1000 flexes.

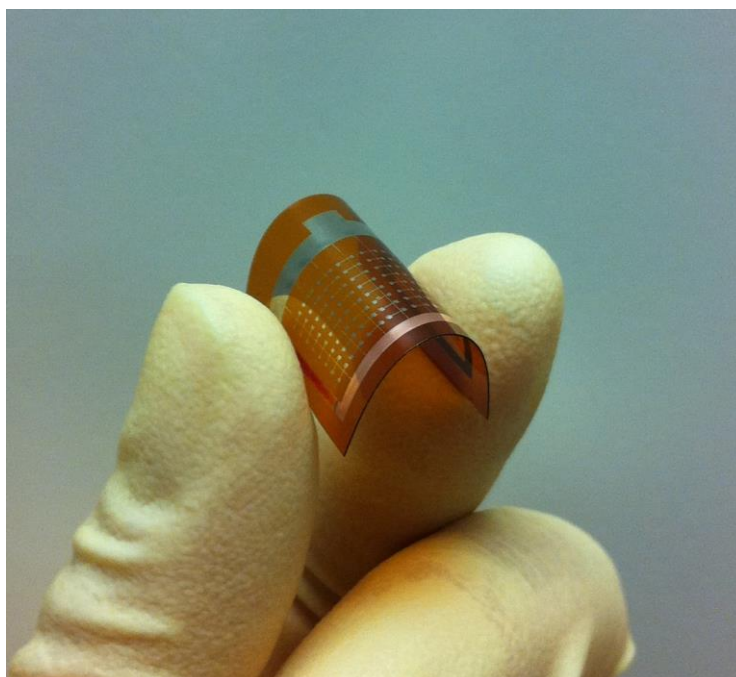


Figure 4.14: The Cu/Cu_xO/Ag ReRAM device was bent into a convex shape.

4.6 Switching Time Tests

Fig 4.15 illustrates the switching time (or writing time) of the SET/RESET operation measured at room temperature. In Fig 4.15(a), a SET voltage of -0.8 V was applied to the top electrode of the memory device. The current that flowed through the cell was recorded as the time changed. It can be observed that a drastic reduction of current happens at a time of approximately 2 s, which means that it takes 2 s to switch the resistance from LRS to HRS. Correspondingly, it takes roughly 1 s to switch from HRS to LRS by applying a RESET voltage of +0.8 V and the result is shown in Fig 4.15(b).

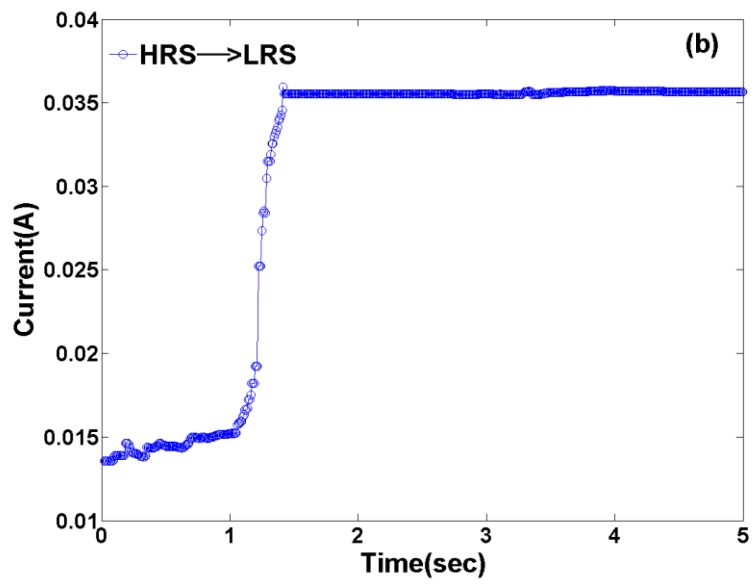
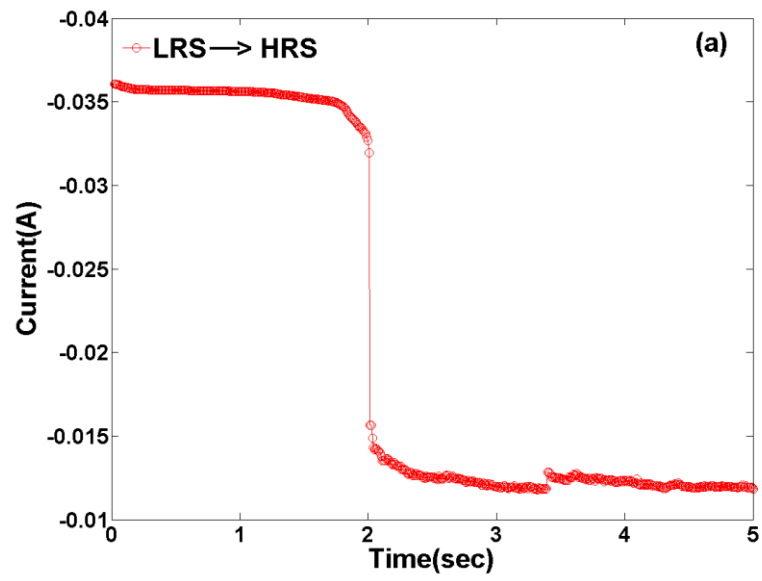


Figure 4.15: Switching time measurements of (a) RET and (b) RESET operation.

To explore the temperature effect and the SET/RESET voltage effect on the switching speed, we conducted the same experiments under different temperatures (from 255 K to 355 K), and applied different SET/RESET voltage biases (from ± 0.6 V to ± 1 V) to switch to the memory cell. However, there was no stable trend for the temperature and voltage bias effects observed. Therefore, no corresponding results are shown in this thesis.

Chapter 5

Resistive Switching Mechanism

5.1 Non-Cu-Oxidation Control Group

Fig 5.1 shows the I-V curve of a Cu/Cu_xO/Ag ReRAM device. Compared to these fully fabricated devices, we fabricated a subset of devices without the Cu oxidation procedure and tested the I-V characteristics, which is shown in Fig 5.2. We note that the resistance of devices without Cu oxidation does not show BRS. Furthermore, -0.8 V and +0.8 V were applied to the device as the SET voltages and RESET voltages, switching both the fully fabricated device and the non-oxidation device to HRS and LRS, respectively. The resistances of HRS and LRS were recorded at a low voltage range from -0.01 V to +0.01 V. The results for the fully fabricated device and the no-oxidation device are shown in Fig 5.3(a) and Fig 5.3(b). We noted that the fully fabricated Cu/Cu_xO/Ag ReRAM device shows HRS and LRS with a ratio of 20. However, during the 50 switching cycles, no resistance difference can be confirmed when writing the no-oxidation device to the SET voltage and the RESET voltage.

In conclusion, the Cu oxidation process is necessary for realization of our devices. This also provides some insight into the physical mechanism occurring in these devices that leads to BRS.

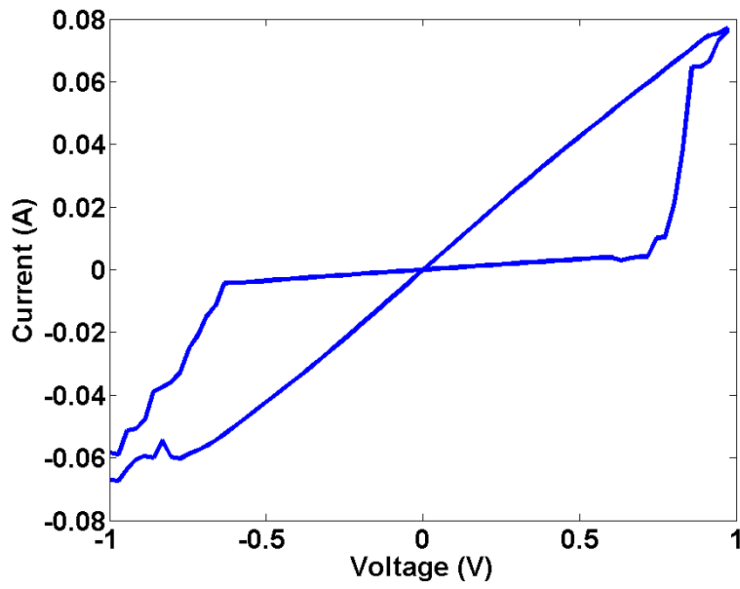


Figure 5.1: Hysteretic I-V behavior of the Cu/Cu_xO/Ag ReRAM device.

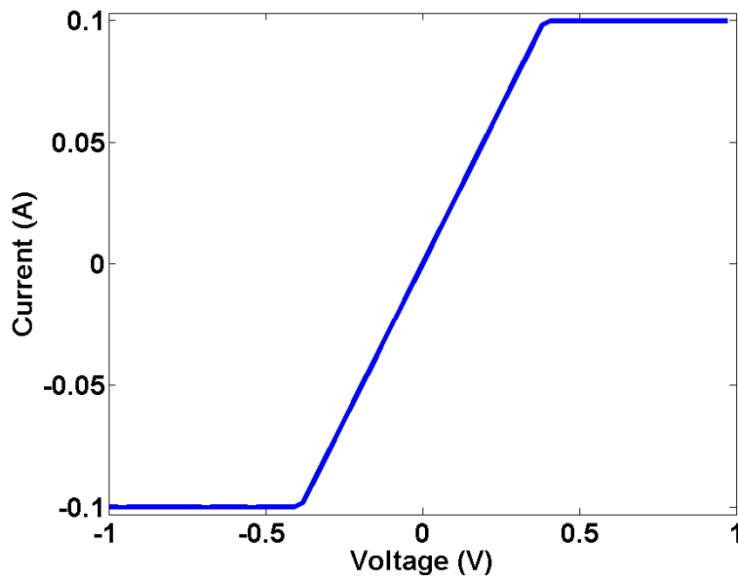


Figure 5.2: I-V curve of a non-oxidation device.

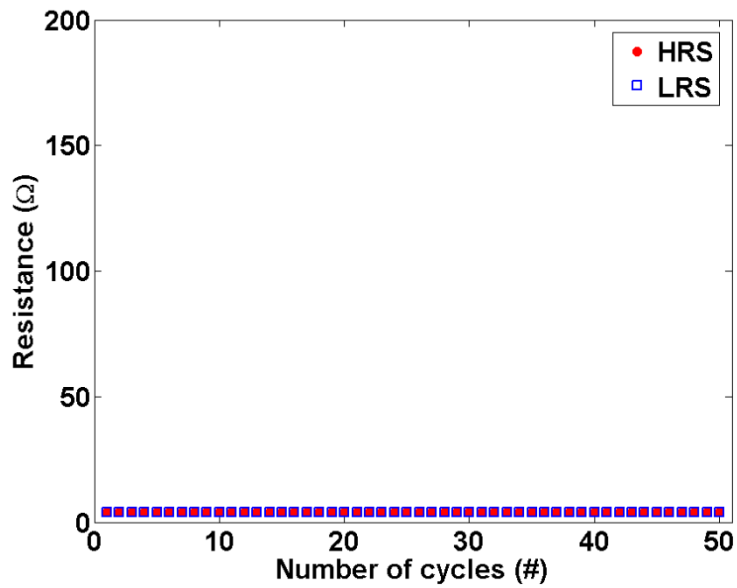
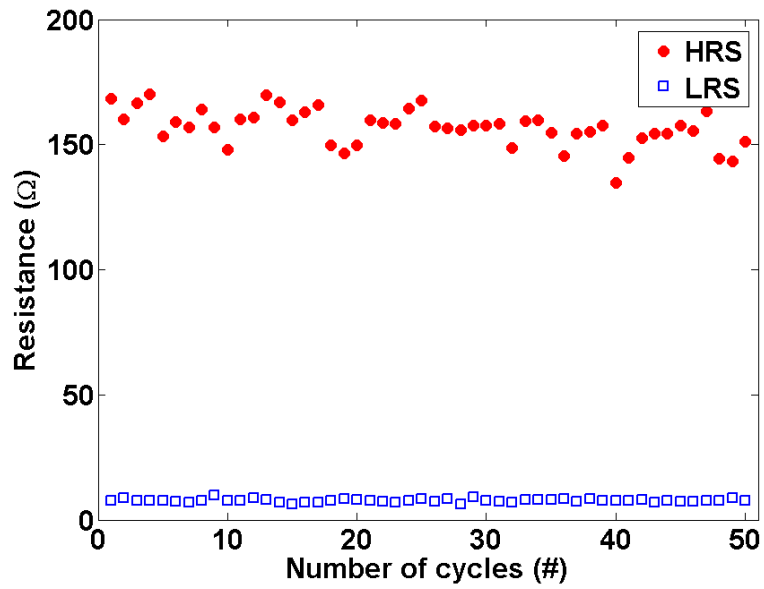


Figure 5.3: Resistance dependence of HRS and LRS on number of switching cycles. (a) A fully fabricated Cu/Cu_xO/Ag ReRAM device. (b) A Cu/Ag device without Cu oxidation step.

5.2 Physical Mechanism of Cu/Cu_xO/Ag ReRAM Devices

Temperature-dependent resistance measurements on Cu/Cu_xO/Ag ReRAM devices were performed to explore the physics of the resistive switching conduction mechanism.

The resistance of devices at initial resistance state (IRS, resistance state before electroforming), HRS and LRS as a function of temperature is shown in Fig 5.4. The temperature range is from 255 K to 355 K with a step size of 15 K. Reproducible BRS can be observed in this temperature range. The resistance of all states is read by sweeping the voltage bias in a small range from -0.01 V to +0.01 V to prevent the device from switching to a different resistive state. The IRS and HRS can be considered to exhibit semiconductor behavior because when the temperature increases, the resistance of the device decreases. On the contrary, a weak metallic behavior can be observed at LRS. There is potential possibility that the filamentary conductive paths were generated in the RESET process, which results in very low resistance. However, the rupture of conductive filament paths happened at SET process, thus the temperature-dependent HRS is dominated by the semiconductor behavior of the Cu_xO. Furthermore, the ratio of HRS/LRS drops from approximately 82 to 13 over the temperature range from 255 K to 355 K.

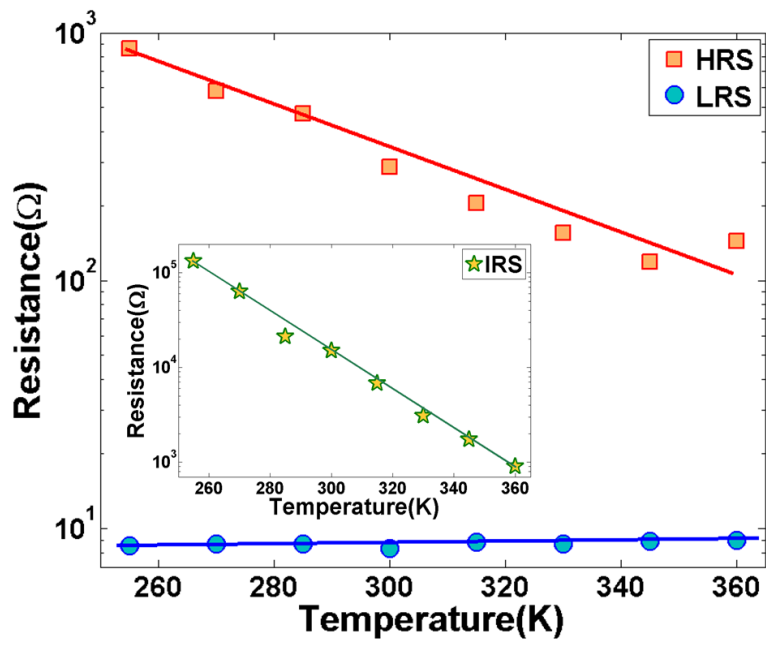


Figure 5.4: Temperature dependence of HRS, IRS and LRS.

To exclude the effect of the SET and RESET operations on the original physical state, the temperature-dependent I-V measurement was conducted after the device was switched to HRS by applying a SET voltage (-0.8 V). Fig 5.5 shows the I-V curves in logarithm scale measured at various temperatures from 255 K to 315 K, which is in a positive voltage region (0 V to +0.5 V) low enough to prevent the RESET process. It was shown that with the increase of temperature, the current increases gradually. The $\ln(I)$ versus $1/KT$ for HRS was plotted in Fig 5.6. The plot shows five generally straight lines at different voltages. Then, the activation energy (E_a) at each voltage bias was calculated from the slopes of fitting lines. Fig 5.7 shows the calculated E_a as a function of applied voltages.

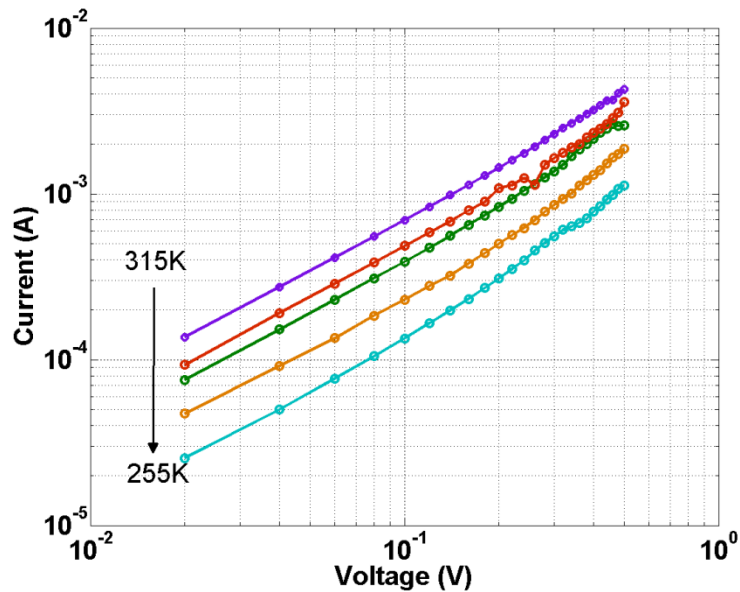


Figure 5.5: Temperature-dependent I-V characteristics at HRS in log-log scale.

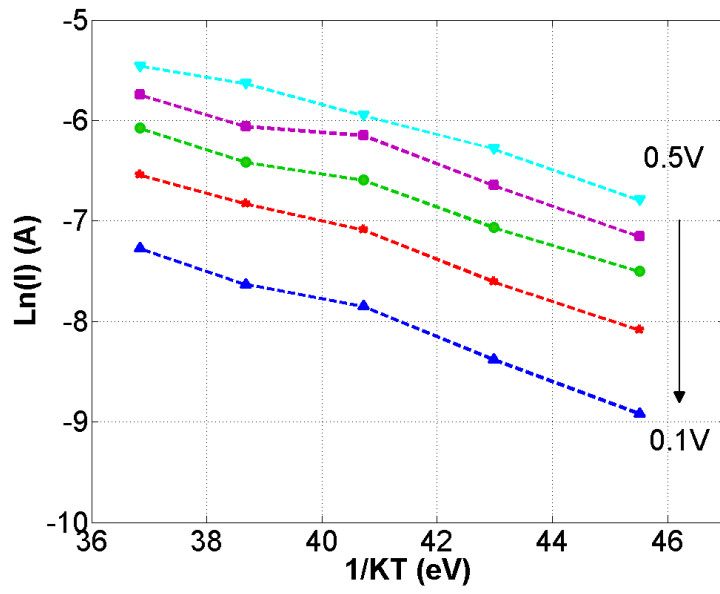


Figure 5.6: The LnI versus 1/KT curve for HRS.

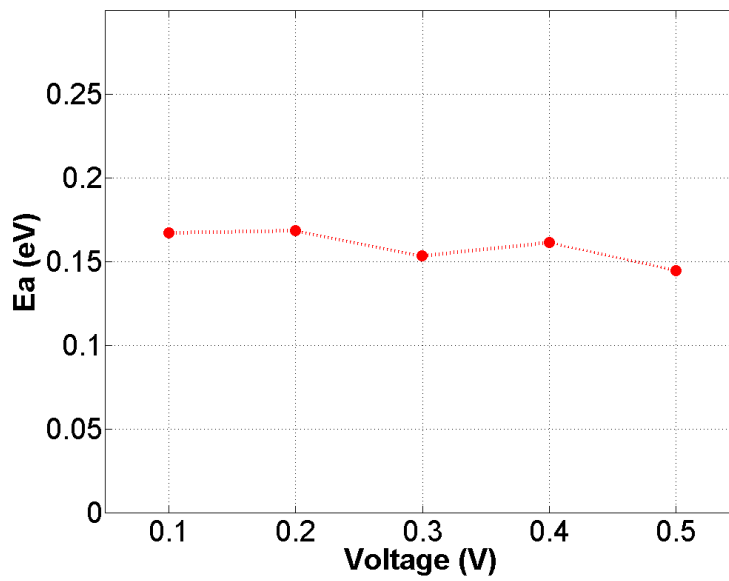


Figure 5.7: Activation energy at various voltages.

To further clarify the resistive switching mechanism of Cu/Cu_xO/Ag memory devices, the double logarithmic plot of I-V curves for the positive region was replotted, which is shown in Fig 5.8. As indicated in Fig 5.8, in the positive voltage bias region, starting from 0 V, the I-V behavior of Cu/Cu_xO/Ag memory cell in HRS is very close to linear and the linear dependence for applied voltage is smaller than +0.60 V. In this low-voltage region, the slope of I-V curve is very close to 1, in agreement with Ohm's law. Next, a dramatic increase of current is observed at approximately +0.8 V (V_{RESET}) due to the formation of conductive filaments through the device [4, 16], which does not follow space charge limited current (SCLC) theory [48]. Finally, the Ohmic conduction behavior was observed again in the decreasing voltage bias scan in the LRS.

Different cell-size ReRAM devices were fabricated. The cell sizes were from 20×20 μm² to 800×800 μm², which is shown in Fig 5.9. Fig 5.10 shows the cell-size dependence of the HRS and LRS of Cu/Cu_xO/Ag memory cells. Different cell-size Cu/Cu_xO/Ag memory devices were fabricated in the same condition. All devices show BRS during DC voltage scan. The best linear fitting lines are also shown in the figure. With the increase of cell size, the ratio of HRS/LRS decreases roughly from 30 to 10. The resistance of HRS decreases from approximately 264 Ω to 46 Ω, whereas the resistance of LRS only shows slight dependence of cell sizes, decreasing from 8.32 Ω to 4.46 Ω. The result reveals that the resistive switching behavior is a local phenomenon in the Cu/Cu_xO/Ag memory cell, dominated by the local conductive filament path, further indicating the resistive switching mechanism of the Cu/Cu_xO/Ag MOM cross-point structure is attributed to the formation and rupture of the conductive filament paths [16, 49, 50].

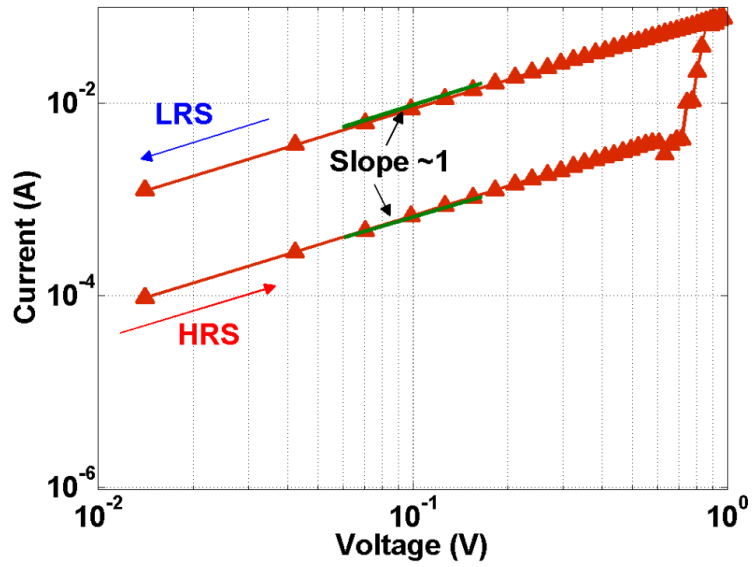


Figure 5.8: Logarithmic plot of I-V characteristic of positive voltage region.

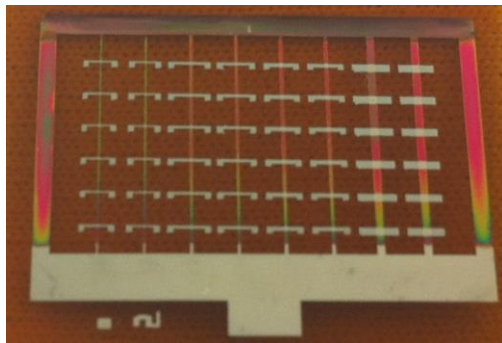


Figure 5.9: Photograph of the fabricated different cell-size ReRAM array.

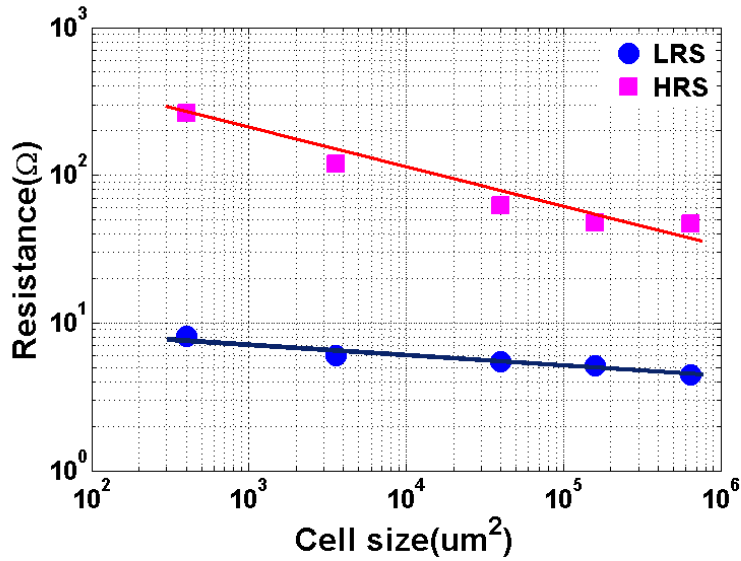


Figure 5.10: Resistance of HRS and LRS versus cell size of Cu/Cu_xO/Ag ReRAM devices.

5.3 Resistive Switching Mechanism Model

Based on the temperature-dependent measurement and cell-size dependent measurement analysis, we are able to conceive an intuitive diagram of the BRS in the device. Fig 5.11 shows the schematic diagram of the resistive switching mechanism model of the Cu/Cu_xO/Ag ReRAM devices. Note that the geometry and distribution of this model are ideally simplified and the actual conduction is considered to be more complicated. Fig 5.11(a) shows the fresh device at IRS. After the electroforming process (Fig 5.11(b)), a strong electrical field leading to the formation of a conductive filament is taking in the insulating matrix between the Ag top electrode and the Cu bottom electrode. Next, at HRS, the filaments are ruptured under a large negative voltage. Consider the SET process, a huge SET current will generate high Joule heating at local filament paths, leading to the rupture of conductive paths, which is shown in Fig 5.11(c). In this case, the carriers can only transport through the semiconductor material Cu_xO thin film, exhibiting a semiconductor behavior. On the other hand, the conductive filament paths are rebuilt

under a certain positive voltage at LRS (Fig 5.11(d)). In this case, the current flowing through the device is mainly confined in conductive filament paths. Thus a metallic behavior is shown at LRS. Note that the SET process and the RESET process are reversible processes, leading to the switching of HRS and LRS in a working device.

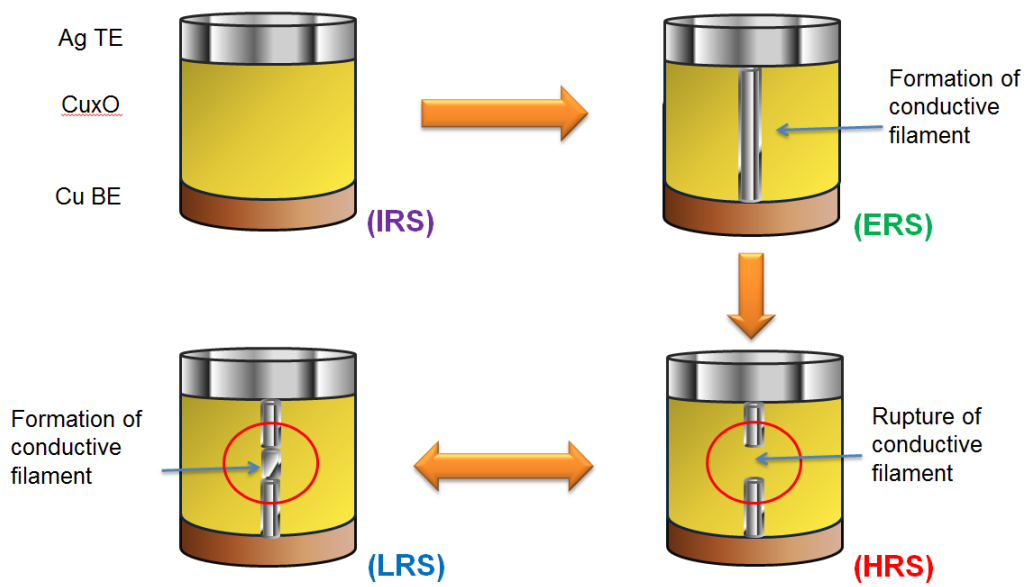


Figure 5.11: Schematic diagram of the resistive switching mechanism model. (a) IRS. (b) ERS. (c) HRS. (d) LRS.

Chapter 6

Conclusion and Future Work

In this work, we discussed the design and fabrication of the Cu/Cu_xO/Ag ReRAM device. We described the process for fabricating ReRAM devices. We used ink-jet printing technology during the fabrication process which has great potential for roll-to-roll processing in the industrial production. The temperature of entire fabrication process was under 200 °C. The memory devices were fabricated based on Cu and Ag, which are abundant and easy to process. The electroformed devices exhibited reproducible and reliable BRS characteristics under a temperature range from 255 K to 355 K. The fabricated device showed good switching endurance (more than 100 cycles), excellent data retention performance (nearly 2 weeks). In addition, as a flexible device, the device had great mechanical robustness properties.

The temperature-dependent and cell-size dependent measurement results reveal that the physical mechanism of the memory device is attributed to the formation and rupture of the local conductive filament paths in the insulating matrix between two electrodes. The device shows semiconductor-like behavior at HRS and IRS, and exhibits metallic behavior at LRS. Moreover, a physical mechanism model of the device has been presented. The observed trend of increased ratio of HRS to LRS as the cell area decreases can be regarded as a benefit of device scaling. The simple, flexible inexpensive low-temperature-fabricated low-voltage operation ink-jet printed Cu/Cu_xO/Ag memory cell is expected to provide opportunities for flexible memory electronics and neuromorphic electronic devices.

In terms of future work, we are studying various methods to optimize the fabrication process to increase the ratio of HRS/LRS and decrease the writing time. Possible solutions include: oxidizing high-quality Cu_xO and decreasing the memory cell size. Our current approach using an oxidation temperature of $200\text{ }^\circ\text{C}$ gets a layer of Cu_xO with a thickness of approximately 23 \AA . In addition, since the smallest deposit feature limit of the cartridge is $20\text{ }\mu\text{m}\times 20\text{ }\mu\text{m}$, a smaller cell size needs a brand-new design utilizing photolithography technology to be achieved. Moreover, we are in the process of measuring the low frequency noise (flicker noise or $1/f$ noise), which will be a useful tool and offer new ideas in understanding the operation mechanism of the ReRAM devices.

References

- [1] Lee, Seunghyup, Heejin Kim, Jinjoo Park, and Kijung Yong, "Coexistence of unipolar and bipolar resistive switching characteristics in ZnO thin films." *Journal of Applied Physics*, vol. 108, no. 7, pp. 076101, 2010.
- [2] Stewart, D. R., D. A. A. Ohlberg, P. A. Beck, Y. Chen, R. Stanley Williams, Jan Oskar Jeppesen, K. A. Nielsen, and J. Fraser Stoddart, "Molecule-independent electrical switching in Pt/organic monolayer/Ti devices." *Nano Letters*, vol. 4, no. 1, pp. 133-136, 2004.
- [3] Gergel-Hackett, Nadine, Behrang Hamadani, Barbara Dunlap, John Suehle, Curt Richter, Christina Hacker, and David Gundlach, "A flexible solution-processed memristor." *Electron Device Letters, IEEE*, vol. 30, no. 7, pp. 706-708, 2009.
- [4] Han, Jin-Woo, and M. Meyyappan, "Copper oxide resistive switching memory for e-textile." *AIP Advances*, vol. 1, no. 3, pp. 032162, 2011.
- [5] Guan, Weihua, Ming Liu, Shibing Long, Qi Liu, and Wei Wang, "On the resistive switching mechanisms of Cu/ZrO₂: Cu/Pt." *Applied Physics Letters*, vol. 93, no. 22, pp. 223506, 2008.
- [6] Liu, Qi, Weihua Guan, Shibing Long, Rui Jia, Ming Liu, and Junning Chen, "Resistive switching memory effect of ZrO₂ films with Zr⁺ implanted." *Applied physics letters*, vol. 92, no. 1, pp. 012117-012117, 2008.

- [7] Fujii, T., M. Kawasaki, A. Sawa, H. Akoh, Y. Kawazoe, and Y. Tokura, "Hysteretic current–voltage characteristics and resistance switching at an epitaxial oxide Schottky junction $\text{SrRuO}_3/\text{SrTi}_{0.99}\text{Nb}_{0.01}\text{O}_3$." *Applied Physics Letters*, vol. 86, no. 1, pp. 012107-012107, 2005.
- [8] Williams, R, "How we found the missing memristor." *Spectrum, IEEE*, vol. 45, no. 12, pp. 28-35, 2008.
- [9] Mikolajick, T., C. Dehm, W. Hartner, I. Kasko, M. J. Kastner, N. Nagel, M. Moert, and C. Mazure, "FeRAM technology for high density applications." *Microelectronics Reliability*, vol. 41, no. 7, pp. 947-950, 2001.
- [10] Tehrani, S., E. Chen, M. Durlam, T. Zhu, and H. Goronkin, "High density nonvolatile magnetoresistive RAM." In *Proceeding International Electron Devices Meeting*, pp. 8-11. 1996.
- [11] Wong, H-SP, Simone Raoux, SangBum Kim, Jiale Liang, John P. Reifenberg, Bipin Rajendran, Mehdi Asheghi, and Kenneth E. Goodson, "Phase change memory." *Proceedings of the IEEE*, vol. 98, no. 12, pp. 2201-2227, 2010.
- [12] Hickmott, T. W, "Low-Frequency Negative Resistance in Thin Anodic Oxide Films." *Journal of Applied Physics*, vol. 33, no. 9, pp. 2669-2682, 2004.
- [13] Oka, Keisuke, Takeshi Yanagida, Kazuki Nagashima, Hidekazu Tanaka, and Tomoji Kawai, "Nonvolatile bipolar resistive memory switching in single crystalline NiO heterostructured nanowires." *Journal of the American Chemical Society*, vol. 131, no. 10, pp. 3434-3435, 2009.

- [14] Panda, D., A. Dhar, and S. K. Ray, "Nonvolatile and unipolar resistive switching characteristics of pulsed laser ablated NiO films." *Journal of Applied Physics*, vol.108, no. 10, pp. 104513, 2010.
- [15] Chen, Y. S., H. Y. Lee, P. S. Chen, P. Y. Gu, C. W. Chen, W. P. Lin, W. H. Liu et al, "Highly scalable hafnium oxide memory with improvements of resistive distribution and read disturb immunity." In *Electron Devices Meeting (IEDM), 2009 IEEE International*, pp. 1-4. IEEE, 2009.
- [16] Wang, Sheng-Yu, Chin-Wen Huang, Dai-Ying Lee, Tseung-Yuen Tseng, and Ting-Chang Chang, "Multilevel resistive switching in Ti/Cu_xO/Pt memory devices." *Journal of Applied Physics*, vol. 108, no. 11, pp. 114110, 2010.
- [17] Yan, X. B., Y. D. Xia, H. N. Xu, X. Gao, H. T. Li, R. Li, J. Yin, and Z. G. Liu, "Effects of the electroforming polarity on bipolar resistive switching characteristics of SrTiO_{3-δ} films." *Applied Physics Letters*, vol. 97, no. 11, pp. 112101, 2010.
- [18] Lee, Chang Bum, Dong Soo Lee, Anass Benayad, Seung Ryul Lee, Man Chang, Myoung-Jae Lee, Jihyun Hur, Chang Jung Kim, and U-In Chung, "Highly uniform switching of tantalum embedded amorphous oxide using self-compliance bipolar resistive switching." *Electron Device Letters, IEEE*, vol. 32, no. 3, pp. 399-401, 2011.
- [19] Fujimoto, Masayuki, Hiroshi Koyama, Yuji Nishi, and Toshimasa Suzuki, "Resistive switching properties of high crystallinity and low-resistance Pr_{0.7}Ca_{0.3}MnO₃ thin film with point-contacted Ag electrodes." *Applied Physics Letters*, vol. 91, no. 22, pp. 223504-223504, 2007.
- [20] Kim, Hee-Dong, Ho-Myoung An, Kyoung Chan Kim, Yujeong Seo, Ki-Hyun Nam, Hong-Bay Chung, Eui Bok Lee, and Tae Geun Kim, "Large resistive-switching

- phenomena observed in Ag/Si₃N₄/Al memory cells." *Semiconductor Science and Technology*, vol. 25, no. 6, pp. 065002, 2010.
- [21] Chen, Lin, Qing-Qing Sun, Jing-Jing Gu, Yan Xu, Shi-Jin Ding, and David Wei Zhang, "Bipolar resistive switching characteristics of atomic layer deposited Nb₂O₅ thin films for nonvolatile memory application." *Current Applied Physics*, vol. 11, no. 3, pp. 849-852, 2011.
- [22] Younis, Adnan, Dewei Chu, Ionsecu Mihail, and Sean Li, "Interface-Engineered Resistive Switching: CeO₂ Nanocubes as High-Performance Memory Cells." *ACS applied materials & interfaces*, vol. 5, no. 19, pp. 9429-9434, 2013.
- [23] Nagashima, Kazuki, Takeshi Yanagida, Keisuke Oka, Masateru Taniguchi, Tomoji Kawai, Jin-Soo Kim, and Bae Ho Park, "Resistive switching multistate nonvolatile memory effects in a single cobalt oxide nanowire." *Nano letters*, vol. 10, no. 4, pp. 1359-1363, 2010.
- [24] Nagashima, Kazuki, Takeshi Yanagida, Keisuke Oka, and Tomoji Kawai, "Unipolar resistive switching characteristics of room temperature grown SnO₂ thin films." *Applied Physics Letters*, vol. 94, no. 24, pp. 242902, 2009.
- [25] Yoshida, Chikako, Masaki Kurasawa, Young Min Lee, Masaki Aoki, and Yoshihiro Sugiyama, "Unipolar resistive switching in CoFeBMgO/CoFeB magnetic tunnel junction." *Applied Physics Letters*, vol. 92, pp. 113508, 2008.
- [26] Gao, Xu, Yidong Xia, Bo Xu, Jizhou Kong, Hongxuan Guo, Kui Li, Haitao Li et al, "Unipolar resistive switching behaviors in amorphous lutetium oxide films." *Journal of Applied Physics*, vol. 108, no. 7, pp. 074506, 2010.

- [27] Jeong, Doo Seok, Herbert Schroeder, and Rainer Waser, "Coexistence of Bipolar and Unipolar Resistive Switching Behaviors in a Pt/TiO₂/Pt Stack." *Electrochemical and solid-state letters*, vol. 10, no. 8, G51-G53, 2007.
- [28] Zhang, Jian, Hui Yang, Qi-long Zhang, Shurong Dong, and J. K. Luo, "Bipolar resistive switching characteristics of low temperature grown ZnO thin films by plasma-enhanced atomic layer deposition." *Applied Physics Letters*, vol. 102, no. 1, pp. 012113, 2013.
- [29] Shen, Wan, Regina Dittmann, and Rainer Waser, "Reversible alternation between bipolar and unipolar resistive switching in polycrystalline barium strontium titanate thin films." *Journal of Applied Physics*, vol. 107, no. 9, pp. 094506, 2010.
- [30] Lin, Chih-Yang, Chung-Yi Wu, Chen-Yu Wu, Tseung-Yuen Tseng, and Chenming Hu, "Modified resistive switching behavior of ZrO₂ memory films based on the interface layer formed by using Ti top electrode." *Journal of Applied Physics*, vol. 102, no. 9, pp. 094101, 2007.
- [31] Yan, Z. B., S. Z. Li, K. F. Wang, and J-M. Liu, "Unipolar resistive switching effect in YMn_{1-δ}O₃ thin films." *Applied Physics Letters*, vol. 96, no. 1 (2010): pp. 012103-012103.
- [32] Sawa, Akihito, "Resistive switching in transition metal oxides." *Materials today* 11, no. 6, pp. 28-36, 2008.
- [33] Simmons, J. G., and R. R. Verderber, "New conduction and reversible memory phenomena in thin insulating films." *Proceedings of the Royal Society of London. Series A. Mathematical and Physical Sciences*, vol. 301, no. 1464, pp. 77-102, 1967.
- [34] Lee, Myoung-Jae, Seungwu Han, Sang Ho Jeon, Bae Ho Park, Bo Soo Kang, Seung-Eon Ahn, Ki Hwan Kim et al, "Electrical manipulation of nanofilaments in transition-metal oxides for resistance-based memory." *Nano letters*, vol. 9, no. 4, pp. 1476-1481, 2009.

- [35] Choi, B. J., D. S. Jeong, S. K. Kim, C. Rohde, S. Choi, J. H. Oh, H. J. Kim et al, "Resistive switching mechanism of TiO_2 thin films grown by atomic-layer deposition." *Journal of Applied Physics*, vol. 98, no. 3, pp. 033715, 2005.
- [36] Guan, Weihua, Ming Liu, Shibing Long, Qi Liu, and Wei Wang, "On the resistive switching mechanisms of $\text{Cu/ZrO}_2\text{:Cu/Pt}$." *Applied Physics Letters*, vol. 93, no. 22, pp. 223506, 2008.
- [37] Baikalov, A., Y. Q. Wang, B. Shen, B. Lorenz, S. Tsui, Y. Y. Sun, Y. Y. Xue, and CWc Chu, "Field-driven hysteretic and reversible resistive switch at the $\text{Ag-Pr}_{0.7}\text{Ca}_{0.3}\text{MnO}_3$ interface." *Applied Physics Letters*, vol. 83, no. 5, pp. 957-959, 2003.
- [38] Sawa, A., T. Fujii, M. Kawasaki, and Y. Tokura, "Interface resistance switching at a few nanometer thick perovskite manganite active layers." *Applied physics letters*, vol. 88, no. 23, pp. 232112-232112, 2006.
- [39] Hickmott, T. W, "Impurity conduction and negative resistance in thin oxide films." *Journal of Applied Physics*, vol. 35, no. 7, pp. 2118-2122, 2004.
- [40] Cowley, A. M., and S. M. Sze, "Surface States and Barrier Height of Metal-Semiconductor Systems." *Journal of Applied Physics*, vol. 36, no. 10, pp. 3212-3220, 2004.
- [41] Kim, Sungho, Oktay Yarimaga, Sung-Jin Choi, and Yang-Kyu Choi, "Highly durable and flexible memory based on resistance switching." *Solid-State Electronics*, vol. 54, no. 4, pp. 392-396, 2010.
- [42] Ji, Yongsung, Byungjin Cho, Sunghoon Song, Tae Wook Kim, Minhyeok Choe, Yung Ho Kahng, and Takhee Lee, "Stable switching characteristics of organic nonvolatile memory on a bent flexible substrate." *Advanced Materials*, vol. 22, no. 28, pp. 3071-3075, 2010.

- [43] Zou, S., P. Xu, and M. C. Hamilton, "Resistive switching characteristics in printed Cu/CuO/(AgO)/Ag memristors." *Electronics Letters*, vol. 49, no. 13, pp. 829-830, 2013.
- [44] Biesinger, Mark C., Leo WM Lau, Andrea R. Gerson, and Roger St C. Smart, "Resolving surface chemical states in XPS analysis of first row transition metals, oxides and hydroxides: Sc, Ti, V, Cu and Zn." *Applied Surface Science*, vol. 257, no. 3, pp. 887-898, 2010.
- [45] Gibbons, J. F., and W. E. Beadle, "Switching properties of thin NiO films." *Solid-State Electronics*, vol. 7, no. 11, pp. 785-790, 1964.
- [46] Jeong, Doo Seok, Reji Thomas, R. S. Katiyar, J. F. Scott, H. Kohlstedt, A. Petraru, and Cheol Seong Hwang, "Emerging memories: resistive switching mechanisms and current status." *Reports on Progress in Physics*, vol. 75, no. 7, pp. 076502, 2012.
- [47] Zou, S. and M. C. Hamilton, "Flexible non-volatile Cu/Cu_xO/Ag ReRAM memory devices fabricated using ink-jet printing technology," presented at IEEE ECTC, 2014, Orlando, FL, May 27-30, 2014.
- [48] Dong, R., D. S. Lee, W. F. Xiang, S. J. Oh, D-J. Seong, S. H. Heo, H. J. Choi et al, "Reproducible hysteresis and resistive switching in metal-Cu_xO-metal heterostructures." *Applied physics letters*, vol. 90, no. 4, pp. 042107-042107, 2007.
- [49] Kim, Sungho, Hanul Moon, Dipti Gupta, Seunghyup Yoo, and Yang-Kyu Choi, "Resistive switching characteristics of sol-gel zinc oxide films for flexible memory applications." *Electron Devices, IEEE Transactions on*, vol. 56, no. 4, pp. 696-699, 2009.
- [50] Zou, S. and M. C. Hamilton, "Ink-jet Printed Cu/Cu_xO/Ag ReRAM Memory Devices Fabricated on Flexible Substrates" presented at the MRS Spring Meeting 2014, San Francisco, CA, April 21-25, 2014.

Appendix A
Processing Equipment and Materials

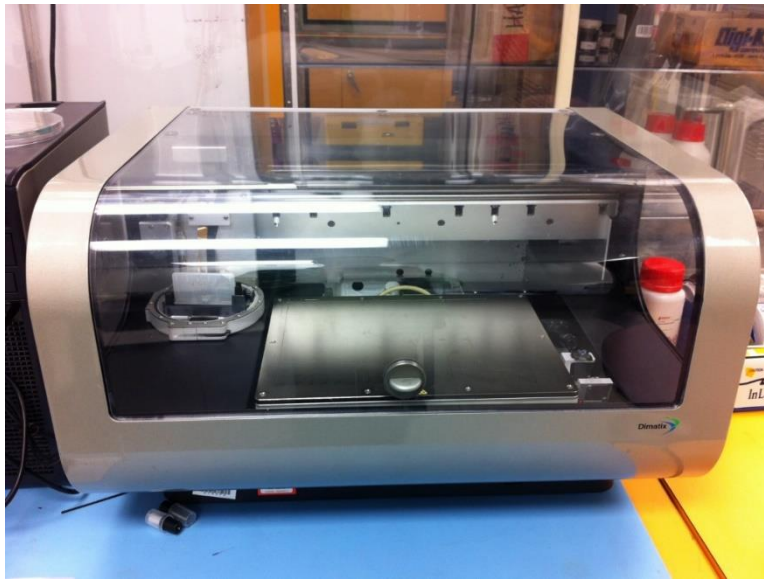


Figure A.1: FUJIFILM Dimatix Material Printer.

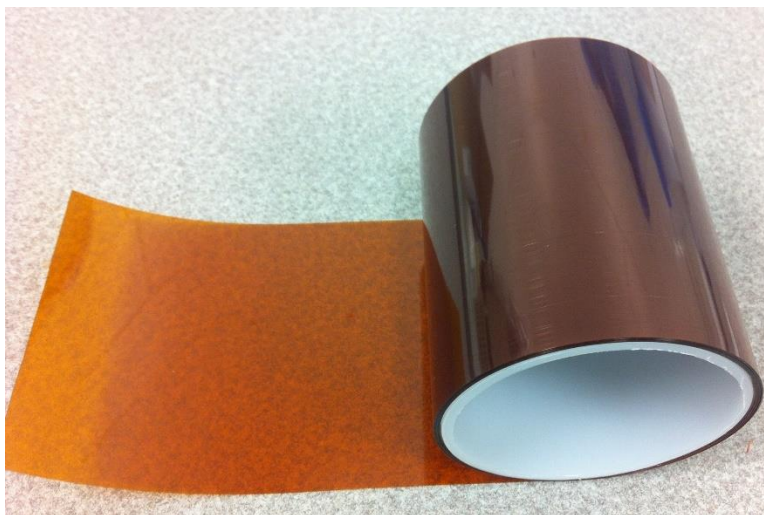


Figure A.2: Kapton polyimide substrate.

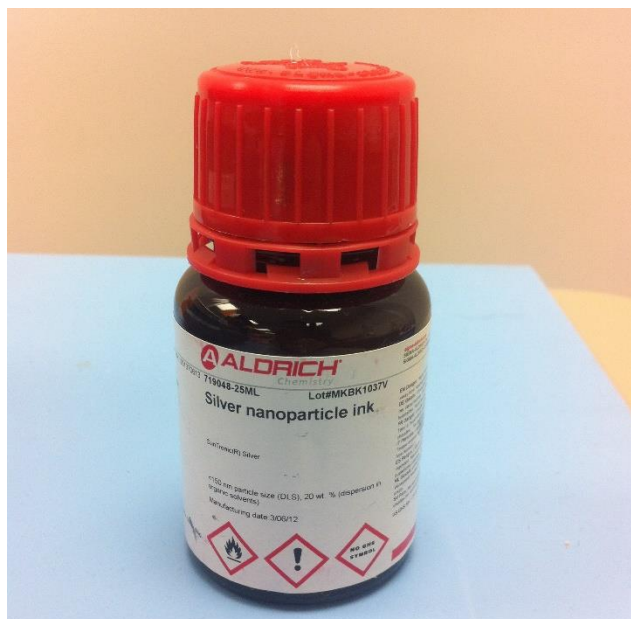


Figure A.3: Silver nanoparticle ink.

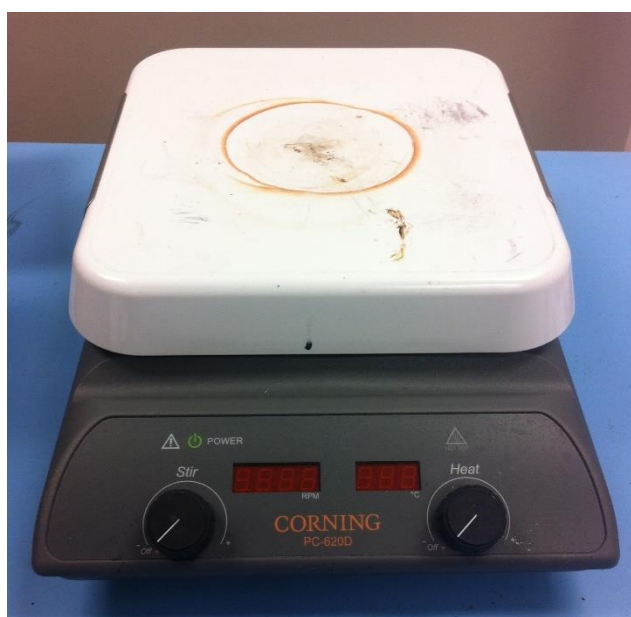


Figure A.4: Hot plate.



Figure A.5: YES (Yield Engineering Systems) vacuum cure oven.

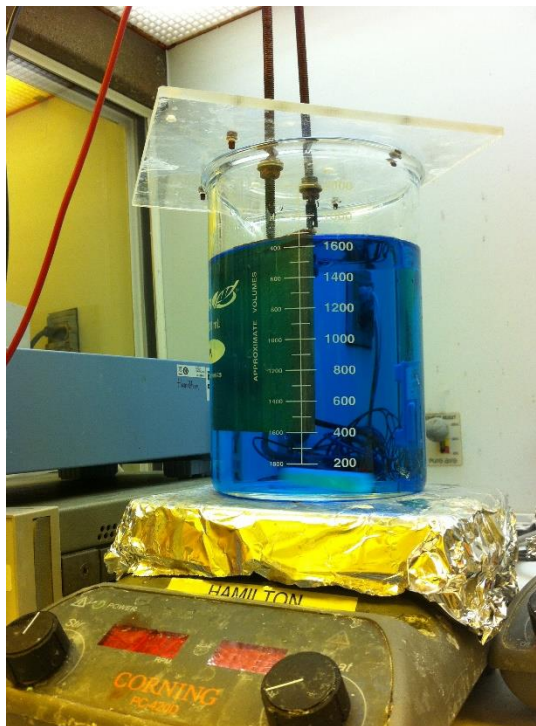


Figure A.6: Copper electroplating equipment.



Figure A.7: Keithley 4200 (Semiconductor Characterization Systems) parameter analyzer.

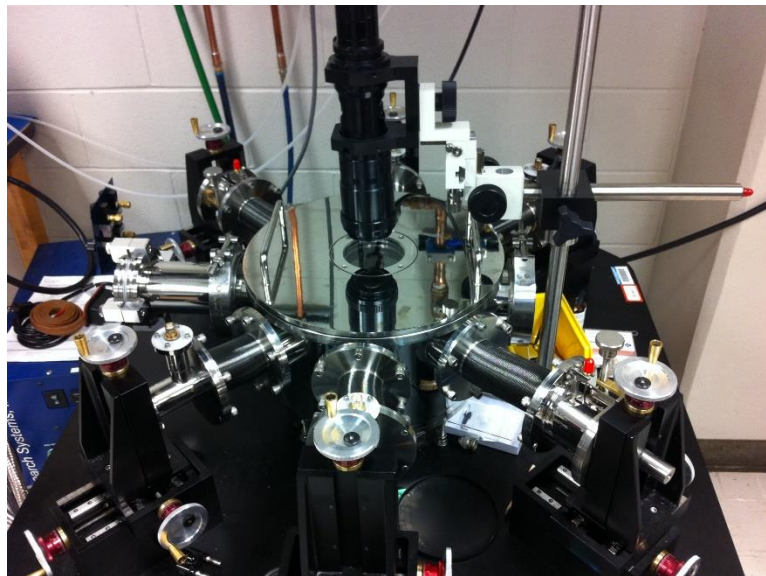


Figure A.8: Micro-manipulated cryogenic probe system.